24 JAN 92

PHYSICAL MODELS OF SPALL ZONE GROUND MOTIONS AND THE DETERMINATION OF SPATIAL DECAY RATES

Brian W Stump
Dept of Geological Sciences
Southern Methodist University
Dallas, TX 75275
and
Thomas A. Weaver
EES-3, MS-C335
Los Alamos National Laboratory
Los Alamos, NM 87545

DISCLAIMER

Portions of this document may be illegible in electronic image products. Images are produced from the best available original document.

ABSTRACT

Spall, the tensile failure of near-surface layers, which is observed above contained explosions, has been identified as a possible secondary seismic source contributing to teleseismic and regional signals. The relative importance of this secondary source can be constrained if the motion field in the spall zone is characterized. Spall zone motions from nuclear explosions detonated above the water table at Pahute Mesa are analyzed to develop these models. Acceleration, velocity, displacement, and dwell time measurements are made from gauges placed directly above the explosion, most often at the free surface. Decay of peak motions are strongly affected by the free surface with little change in amplitude out to a free surface range of 100 $m/kt^{1/3}$ followed by rapid decay beyond. Free surface interactions are assessed with first-order elastic spherical wave calculations that match observed peak velocity decays. These results indicate that the spall zone motions may be strongly affected by the scaled depth of burial of the explosion. Spall zone velocities, displacements and dwell times are compared for consistency with a gravitational model. The data is in agreement with the functional form of theoretical models although observed displacements may be as much as a factor of two to four greater than the model predicts for observed velocities and dwell times. These differences may reflect the continuous nature of the spall process and/or the role of material strength in these phenomena.

INTRODUCTION

The contribution of spall to near-source, regional, and teleseismic ground motion records is dependent on scaling laws for the spall process like those for the spherical explosion. In the case of contained explosions these scaling relations are dependent upon the material in which the explosion is emplaced and the depth below the free surface that the explosion is detonated. Physical processes that occur in the transition from hydrodynamic to plastic to elastic response control these relations which relate the effect of explosion yield to the resulting seismic waveforms. In the case of the secondary spall process important physical processes within the spall zone which result in seismic energy must be identified and incorporated into a secondary seismic source model. The explosion yield as well as near surface material properties must be included in these models so that the quantitative effect of the spall secondary source can be predicted over a wide range of environments.

This paper has two primary purposes. The first is to give details of a preliminary study designed to document relationships between physical processes in the spall zone around explosions and resulting seismic waves. The study is preliminary in that a limited number of explosions have been investigated. Since these events are a subset of a much greater population, which includes substantial differences in emplacement media, scaled depth, and geology, they can only be viewed as specific examples. As analysis expands to a greater number of observations, it is our hope that these *local* conclusions become applicable in a more *global* context with insight into important physical parameters and processes controlling spall and the resulting seismic signature.

The second purpose of this work is to illustrate the importance of the physical model assumed for wave propagation in the interpretation of spall zone data. Spall mass and velocity as expressed in terms of momentum is important in the equivalent elastic seismic source representation (Day et al, 1983; Stump, 1985). Quantification of spall momentum includes the determination of decay rates of ground motion within the spall zone. It will be illustrated that the decay rates can be biased if an improper physical model is applied to the interpretation of the data and thus the seismic source function for spall may be affected as it is extrapolated to new conditions. Synthetic wave propagation models are developed to illustrate these effects.

Spall is defined for this report as the process of tensile failure of near surface layers above a contained explosion. This failure occurs when the superposition of the surface reflection and the tail of the upgoing wave leads to a tensile stress that is greater than the material tensile strength and overburden stress.

Spall zone accelerograms are characterized by an initial compressive wave (positive acceleration), negative one-g-dwell during free-fall (ballistic motion) following failure, and a large spall closure signal (positive acceleration) (Figure 1). Spall has been observed in many different media (Eisler and Chilton, 1964; Rinehart, 1959; and Stump and Reinke, 1984). It is non-linear in that it involves the tensile failure of near surface materials and repartitions upgoing energy from the explosion in both time and space as a result of interaction with the free surface and the earth's gravitational field. It is our proposal that a physically based understanding of spall is necessary to develop a predictive model by which its importance as a secondary source of seismic waves can be assessed in different environments.

Equivalent seismic source models for spall were first proposed by Viecelli (1973). Day et al (1983) pointed out the need to conserve momentum in these models. He argued that for 20 s surface waves conservation of momentum implied that the spall source was unimportant. Day's model was applied to near-source data by Stump (1985) and more recently to regional data by Taylor and Randall (1989) and Taylor et al (1991). The importance of the spall process to near-source and regional seismic data was found to depend on improved characterizations of the spall zone. The higher frequency contents of these near source and regional data sets makes spall a possible important secondary source. Near surface dwell times (ballistic free-fall times) for multiple kiloton explosions are near 1 s as illustrated by the AMARILLO ground zero record (Figure 1) with a dwell time of 0.65 s. Regional and teleseismic waves (Schlittenhardt, 1991) with periods around this characteristic time may be affected by the spall process. The equivalence of a body force and moment tensor representation of spall has been shown by Day and McLaughlin (1991). This model when applied to hard rock ground motion simulations indicates that the spall process makes significant contributions to regional waveforms (Baker and McLaughlin, 1990).

Rudimentary scaling relationships for spall were suggested by Viecelli (1973) and Sobel (1978). Spall mass estimates by these authors are independent of material type and differ by a factor of six:

$$M_S = 1.6 \times 10^9 W \text{ kg (Viecelli)}$$
$$M_S = 9.6 \times 10^9 W \text{ kg (Sobel)}$$

where

W: Yield in kilotons (kt)

These empirical relations suffer from poor resolution of spall depth. In cases where depth can be constrained with instrumentation, spall mass is underestimated by both Sobel and Viecelli (Stump, 1985; Rawson, 1981). The

simplest spall models assume that the process is cylindrically symmetric. A complete four dimensional characterization of the spall process is our goal. This more complete characterization may be necessary in situations where near surface geology and material properties strongly affect symmetry. The cost of instrumentation limits most experiments to simpler two dimensional arrays, often only at the free surface. The bulk of data in this report will be from surface accelerometers. Lack of subsurface data makes resolution of spall depth quite difficult. There are indications that depth effects of the spall source on radiated seismic waves may be strong (Koch and Stump, 1990; Day and McLaughlin, 1990). Spall depth must be taken into account when comparing point force and moment tensor representations of the process.

Seismic waves from this secondary source are dependent not only on spall mass but also the velocity at failure. Escape velocity is directly proportional to the characteristic time of gravitationally controlled processes. Spall velocities and total mass are incorporated in momentum or impulse estimates. Momentum is not imparted to the earth instantaneously since spall initiation, dwell time, and rejoin are not concurrent across the test bed. This spatial effect is illustrated in Figure 1 where acceleration records at free surface ranges of 15m, 258m, and 640m are reproduced for the explosion AMARILLO. Spall initiation time, identified by the start of -1 g dwell, increases with range while spall rejoin, designated by the impulsive rejoin signal, decreases with range. Dwell time decreases from 0.65 to 0.25 s over the observational range. Timing variations will produce an equivalent seismic source function which is smoothed in comparison to a point impulse source with equivalent total momentum. These spatial effects result in equivalent point force source spectra which decay at high frequencies as fast as f^{-4} (Stump, 1985). Since the moment tensor is related to the second time derivative of the point force representation, the high frequency decay of the moment tensor representation would be f^{-2} like that predicted by the Mueller-Murphy explosion source function. A purely gravitationally controlled process would predict no static displacement and thus a decaying long period response. Conservation of momentum implies spectra which decay with increasing period (no contribution to 20 s surface waves). Seismic source spectra for the spall process are peaked with the secondary source having its greatest contribution to seismic waves at frequencies near this peak.

Patton (1990) has recognized deficiencies in existing scaling laws and made spall mass and impulse estimates for explosions at Pahute Mesa. Particular consideration of emplacement and spall zone materials, spall timing, and frequency content of the spall signature is needed. Since near-source, regional, and teleseismic waveforms contain frequencies from tenths to tens of Hertz, the frequency band to which spall contributes must be identified.

AMARILLO FREE SURFACE ACCELERATIONS

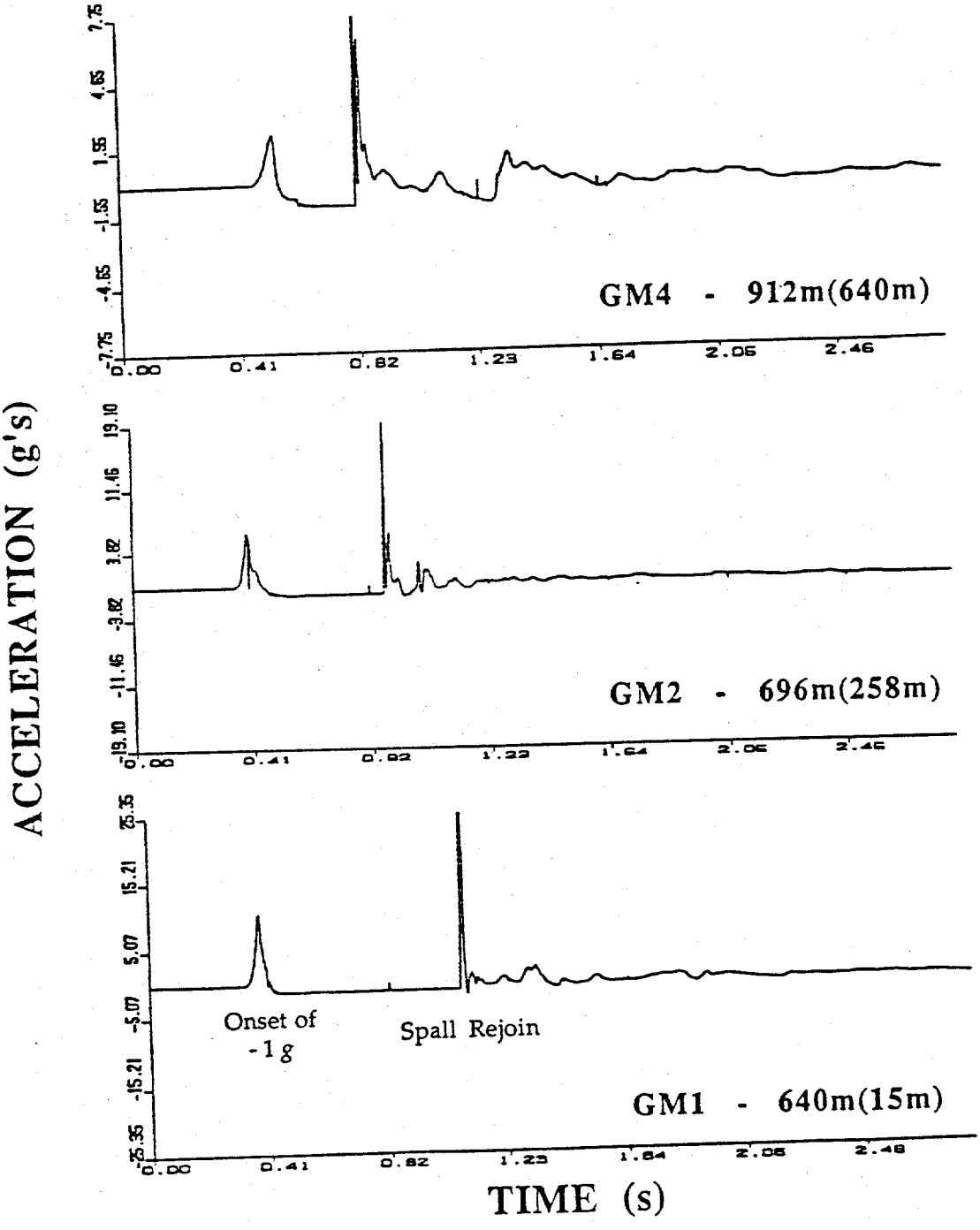

Figure 1: Three, free surface vertical acceleration records from the nuclear explosion AMARILLO. The slant and free surface range (parenthesis) are given for each record.

One must characterize the motion field within the spall zone in order to quantify this secondary seismic source. Some of the earliest estimates of free-field motion decay rates in alluvium, tuff, granite, and salt were summarized by Wheeler and Preston (1968). More recently the free-field data has been characterized by Perret and Bass (1975). Their analysis focused on attenuation rates of acceleration, velocity, and displacements from nuclear explosions in dry alluvium, dry tuff, wet tuff, and hard rock (granite, salt, dolomite and other similar sedimentary rocks). This study included more complete data sets than those utilized earlier by Wheeler and Preston. Both studies focused on the attenuation of waveforms with scaled slant range (SSR) , range (SR) being scaled by the cube root of explosive yield:

$$R' = R/W^{1/3}$$

The ground motions are also appropriately scaled according to the cube root of yield.

The majority of ground motion records from within the spall zone have been made at the free surface and thus free-field decay curves may not be strictly applicable to the data. Bernreuter (1970) developed a set of decay curves for free surface data as well as Weaver (personal communication). Both these representations characterize the amplitude decay in terms of SR, the total distance the wave propagates.

$$\text{Amplitude} \rightarrow R^{-\gamma}$$

An alternate interpretation of the data is characterization of amplitude decay in terms of distance from ground zero (GZ) , r (free surface range - FSR). In the case of surface wave studies the amplitude decay is most often represented in terms of an exponential decay:

$$\text{Amplitude} \rightarrow e^{-\gamma r}$$

Alternatively the data can be described in terms of a power law retaining the free surface range:

$$\text{Amplitude} \rightarrow r^{-\gamma}$$

These last models assume that the free surface plays the dominate role in controlling the close-in velocity observations.

The physical importance of SR and FSR to the interpretation of the observational data will be considered. Two competing processes may be operating, the free surface interaction and the decay of the wavefield with propagation range. At relatively great source to receiver distances the difference between FSR (r) and SR (R) is negligible and, as expected, the two representations converge. Directly above the source the two measures are different and each leads to its own representation of the ground motion.

OBSERVATIONAL DATA

Los Alamos National Laboratory (LANL) routinely makes three-component free surface digital acceleration measurements within the spall zone of contained nuclear tests. Spectral characteristics of the spall secondary source can be constrained with this digital data. Velocity and displacement records are derived from the raw accelerograms. Standard accelerogram corrections for static offsets can be made interactively to reduce bias in velocity and displacement estimates.

Analysis has begun on this observational data base. For illustrative purposes we have included six events detonated above the static water table in Area 19, Pahute Mesa. The experiments include CHANCELLOR (9/01/83), CYBAR (7/17/86), BACKBEACH (4/11/78), NEBBIOLO(6/24/82), SHEEPSHEAD (9/26/79), and AMARILLO (6/27/89).

Free surface accelerometer arrays deployed for three of the shots are reproduced in Figure 2. Three-component accelerometers (in most cases) were installed at each location identified by a closed circle. Typical arrays consisted of instruments at the free surface directly above the explosion (GZ), at a range near 1/2 depth of burial (DOB) (coincides with a recording park), and instruments at 1 DOB. An accelerometer is often located in the emplacement hole so data at depth is available. CHANCELLOR had auxiliary free surface instruments to quantify the change in ground motion across several faults.

CYBAR ACCELEROMETERS

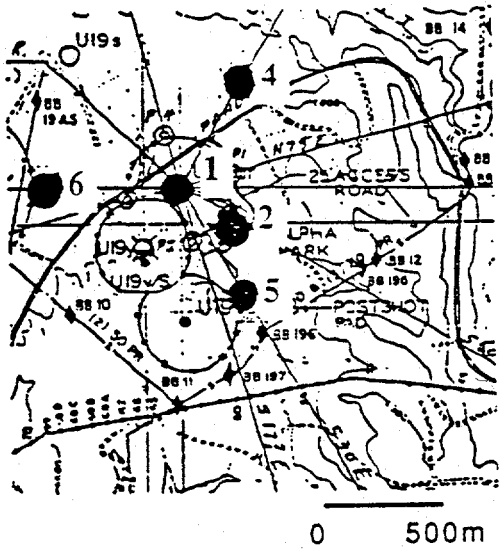

AMARILLO ACCELEROMETERS

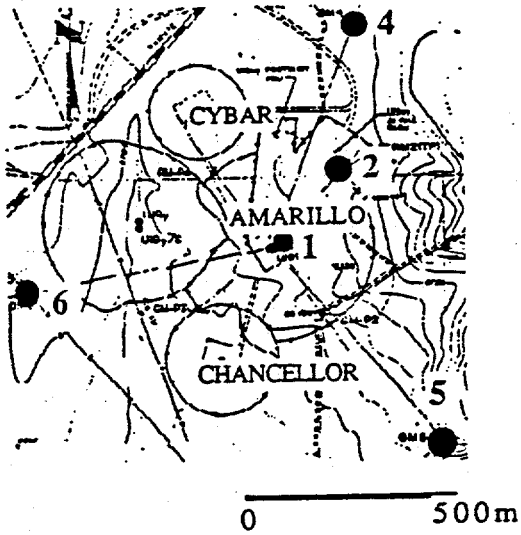

CHANCELLOR ACCELEROMETERS

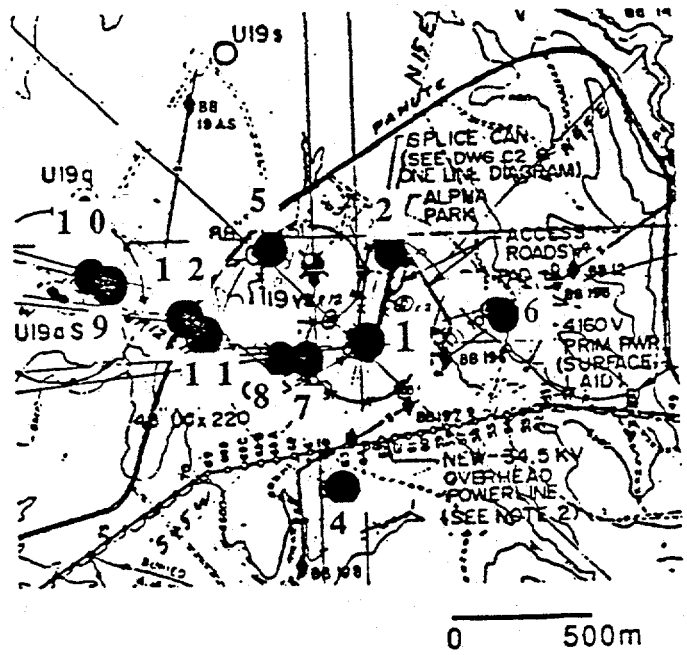

Figure 2: The free surface accelerometer arrays for the nuclear explosions CYBAR, AMARILLO, and CHANCELLOR.

SPALL STUDY METHODOLOGY

SPATIAL DECAYS: Peak vertical accelerations were measured from raw data while peak velocities and displacements were determined from derived waveforms to quantify decay rates for these events. Care was taken to correct for static offsets in acceleration which resulted in ramps in velocity and quadratics in displacement. Spall dwell times were from velocity records (-1g slope) in order to determine average dwell times unaffected by high frequency spikes or noise. Spall criteria follow Stump and Reinke (1984): (1) Minus 1 *g* (allowable range -0.5 to -2.0*g*) vertical acceleration dwell with confirming velocity slope; (2) Moderately impulsive rejoin signals; (3) No horizontal acceleration dwells (<0.2 *g*); (4) Dwell times in excess of 5 ms; and (5) Rejoin amplitudes in excess of 1 *g* . Analysis of velocity records was designed to give average spall estimates that were less affected by local, high frequency variations in acceleration records reflective of noise or local structural effects. Peak vertical velocities prior to spallation were in general greater than 0.7 m/s. This velocity criteria for spall has been applied to the Pahute Mesa spall zone data.

Peak motions were plotted against scaled range to establish decay rates which could be used in developing the equivalent seismic source model. Scaling relations were:

$A' = A*W^{1/3}$	acceleration
$V' = V$	velocity
$D' = D/W^{1/3}$	displacement
$R' = R/W^{1/3}$	distance
$T' = T/W^{1/3}$	dwell time

Free surface data from this study are first plotted against SSR and compared to the other free-field (Wheeler and Preston, 1968; Perret and Bass, 1974) and free surface (Bernrueter,1970; Weaver, personal communication) models in Figures 3a, b, c, d. Data for acceleration, velocity, displacement, and dwell time exhibit clear decays with SSR.

Decay curves of Perret and Bass underestimate the data in acceleration, velocity and to a lessor extent displacement. This result is to be expected since their curves were developed for free-field data. The free surface velocity curve of Bernreuter falls through the upper portions of the data (Figure 3b) as that of Weaver with approximately the correct slope. The acceleration data decays more quickly than Bernreuter (Figure 3a). The Wheeler and Preston free-field curves are in poor agreement with the data. Perret and Bass contains the

Free Surface Accelerations

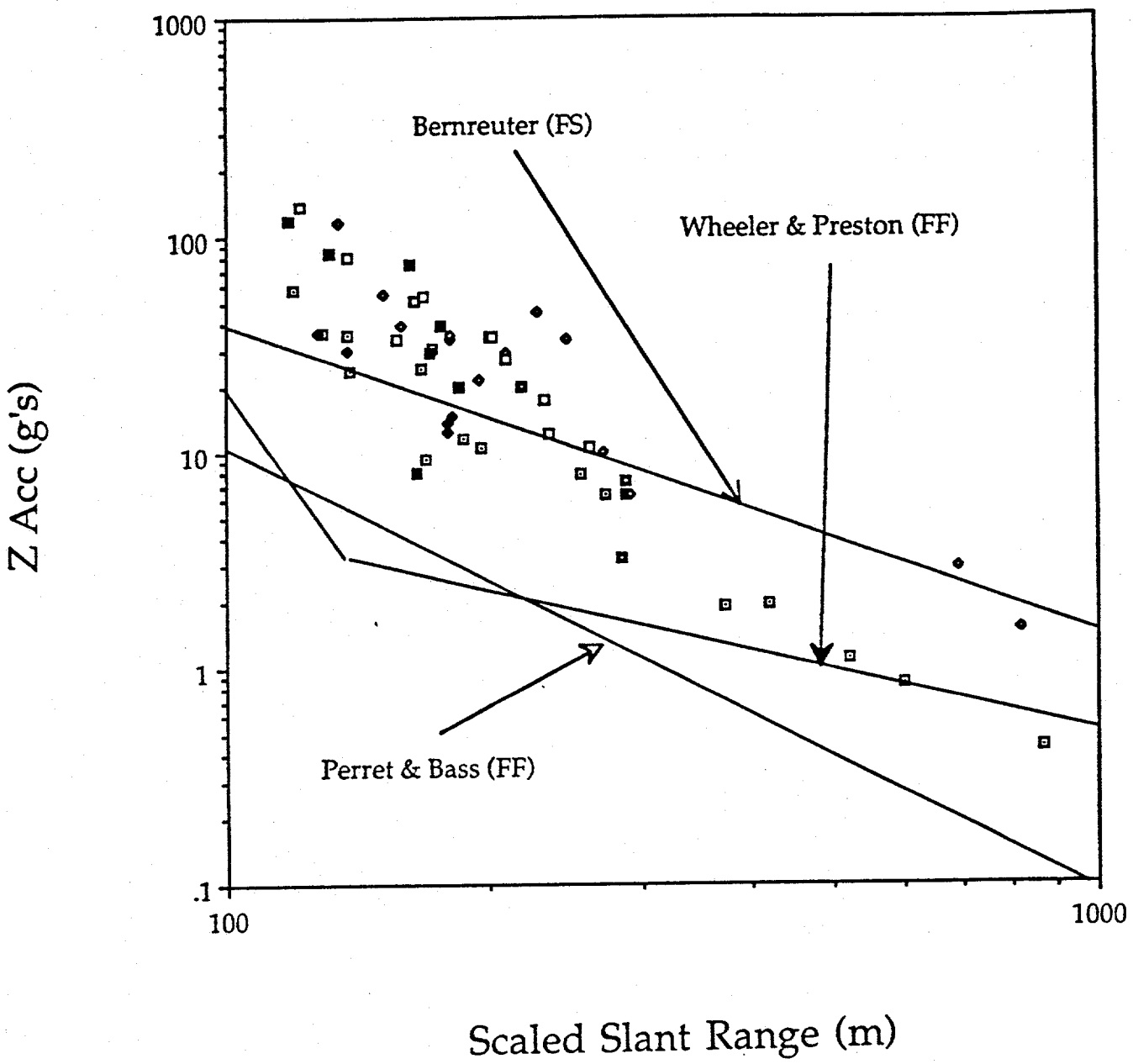

Figure 3a: Scaled free surface peak accelerations from nuclear explosions on Pahute Mesa.

Free Surface Velocities

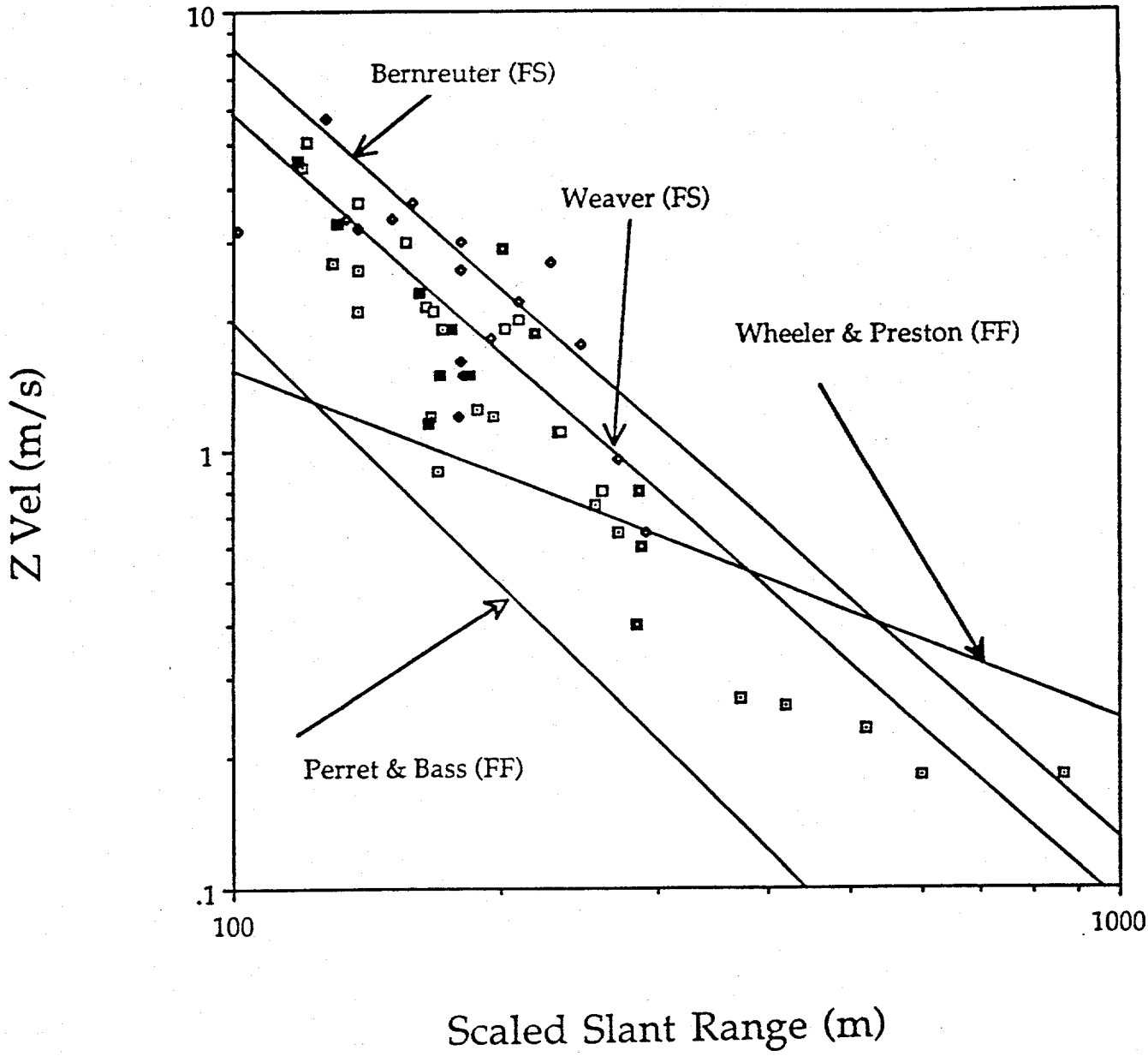

Figure 3b: Free surface peak velocities from nuclear explosions on Pahute Mesa.

Free Surface Displacements

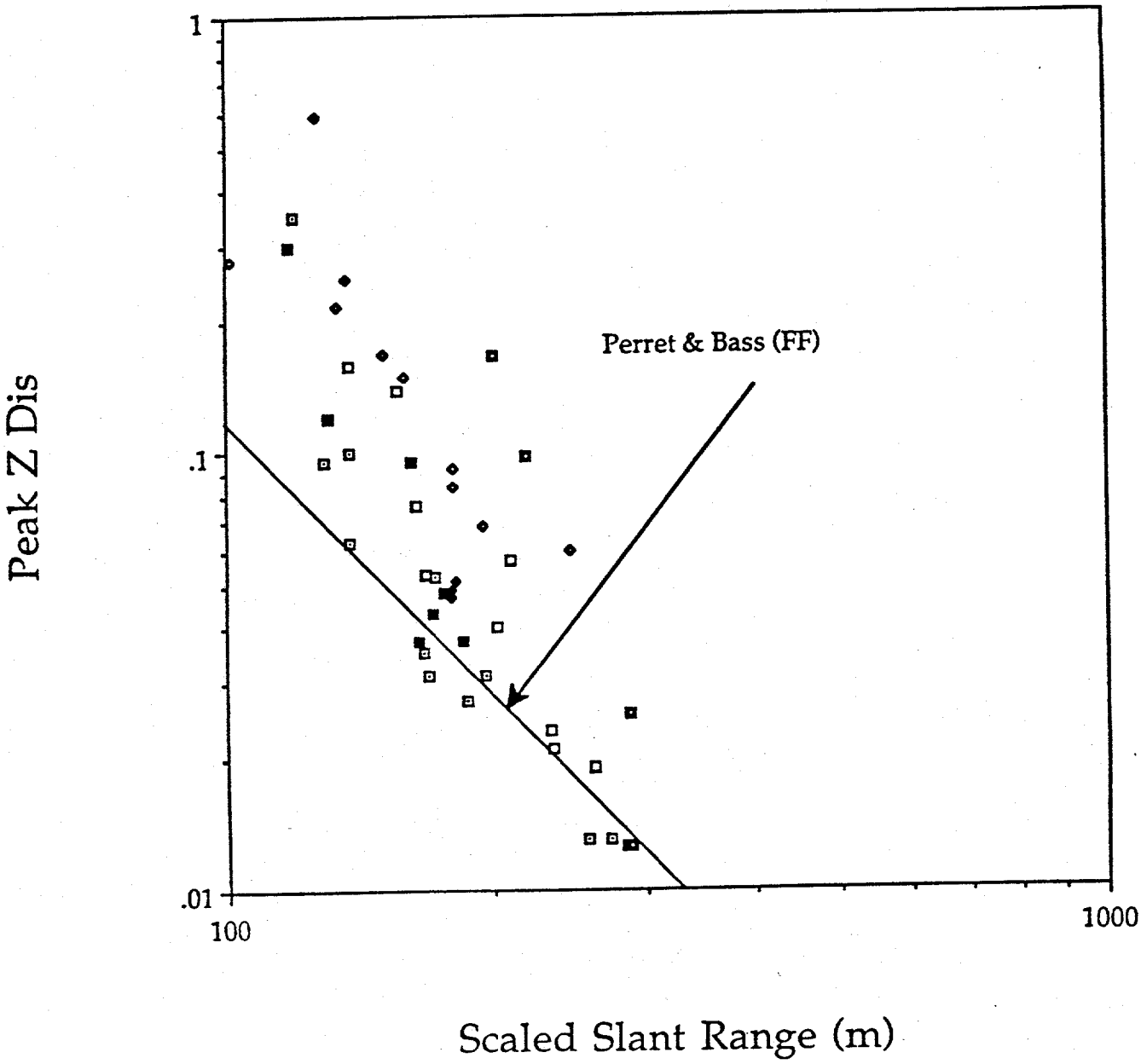

Figure 3c: Scaled free surface peak displacements from nuclear explosions on Pahute Mesa.

Free Surface Dwell Times

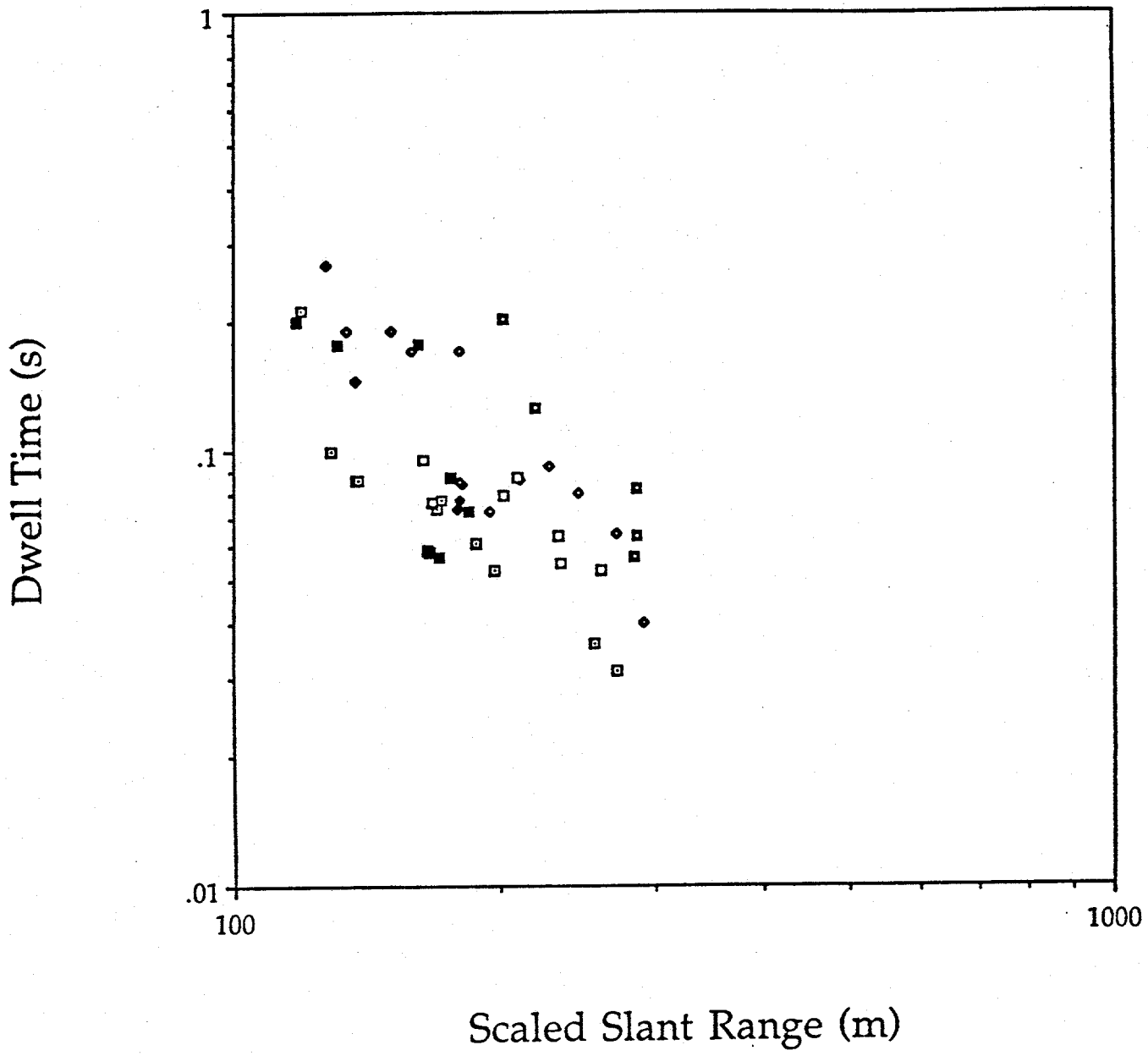

Figure 3d: Scaled free surface spall dwell times from nuclear explosions on Pahute Mesa.

only displacement model for comparison and because it is for free-field data it falls below the data (Figure 3c). Unlike the velocity models, the slope of Perret and Bass displacement curve is less than that of the data.

Decay values were determined for the acceleration, velocity, and displacement data. The value for acceleration was $R^{-2.37}$, velocity $R^{-1.65}$, and displacement $R^{-3.43}$. These values are compared to the models of previous workers in Table 1.

The majority of data recovered by LANL is from the free surface thus simple SSR decays may not be appropriate if boundary effects are important. There is a hint in the data of amplitudes which peak for measurements closest to GZ, directly above the explosion. This focusing towards GZ is strongest for the displacements and is supported by decreased decay rates when GZ data are excluded in fits. Acceleration decay rate decreased from -2.37 to -2.06, velocity from -1.88 to -1.65, and displacement from -3.43 to -2.87. If the free surface effect is important, data can be plotted against FSR. The importance of FSR and SR in interpreting free surface data and attempts to reconcile free surface observations and decay rates (Bernreuter, 1970) with free-field observations (Wheeler and Preston, 1968; Perret and Bass, 1974) are discussed in a later section.

GRAVITATIONAL EFFECTS. Motion measurements displayed in Figures 3 a-c are not independent of one another if dominated by gravitational effects. For a gravity driven model displacement is related to velocity:

$$D = \frac{V^2}{2g}$$

In order to check the consistency of the spall zone data with this simple model peak displacement is plotted against velocity in Figure 4a. The model does not include effects of layers, material properties or medium mechanical response. The relationship predicted by the above equation is designated by open squares. Data follow the trend of these predictions although in most cases the peak displacements are biased high for a given peak spall velocity. The logarithmic plot in Figure 4b indicates that the displacements are as much as a factor of four bigger than predictions throughout the data set. Less than 10% of the data falls below the model predictions while the rest of the data is significantly above the model.

Peak displacement is related to dwell time by:

$$D = \frac{gT^2}{8}$$

Table 1: Observational and Synthetic Decay Laws

Reference	Acceleration	Velocity	Displacement
Perret & Bass (FF)	$R^{-1.92}$	$R^{-1.98}$	$R^{-2.20}$
Bernreuter (FS)	$r^{-1.44}$	$r^{-1.81}$	
Weaver (FS)		$r^{-1.7}$	
Preston & Wheeler (FF)	$R^{-2.9}$ (R<91m) R^{-1} (R>91m)	R^{-4} (R<155m) R^{-1} (R>155m)	
This study data (FS)	$r^{-0.20}$ (r<100m) $r^{-1.96}$ (r>100m)	$r^{-0.13}$ (r<100m) $r^{-1.22}$ (r>100m)	$r^{-0.16}$ (r<100m) $r^{-1.89}$ (r>100m)
This study data (FF)		$R^{-1.88}$ (R<300m) $R^{-1.57}$ (R<2000m)	
This study synthetics (FS)		$r^{-0.15}$ (r<100m) $r^{-1.30}$ (r>100m)	
This study synthetics (FF)		$R^{-1.65}$ (R<560m)	

PAHUTE MESA SPALL DATA

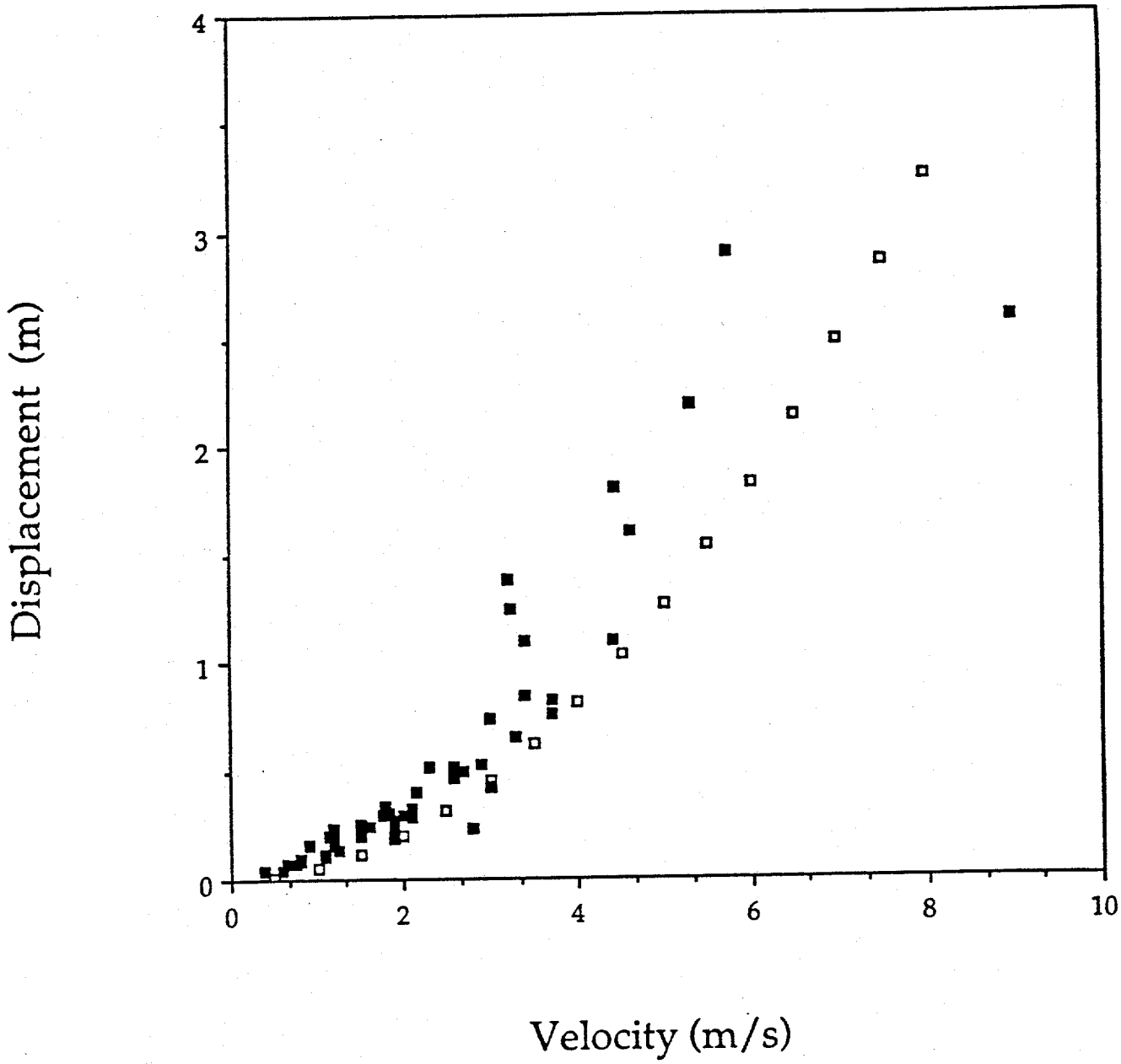

Figure 4a: Comparative plot of peak velocity and displacement from nuclear explosions on Pahute Mesa. A purely gravitational spall model predicts the open squares.

PAHUTE MESA SPALL DATA

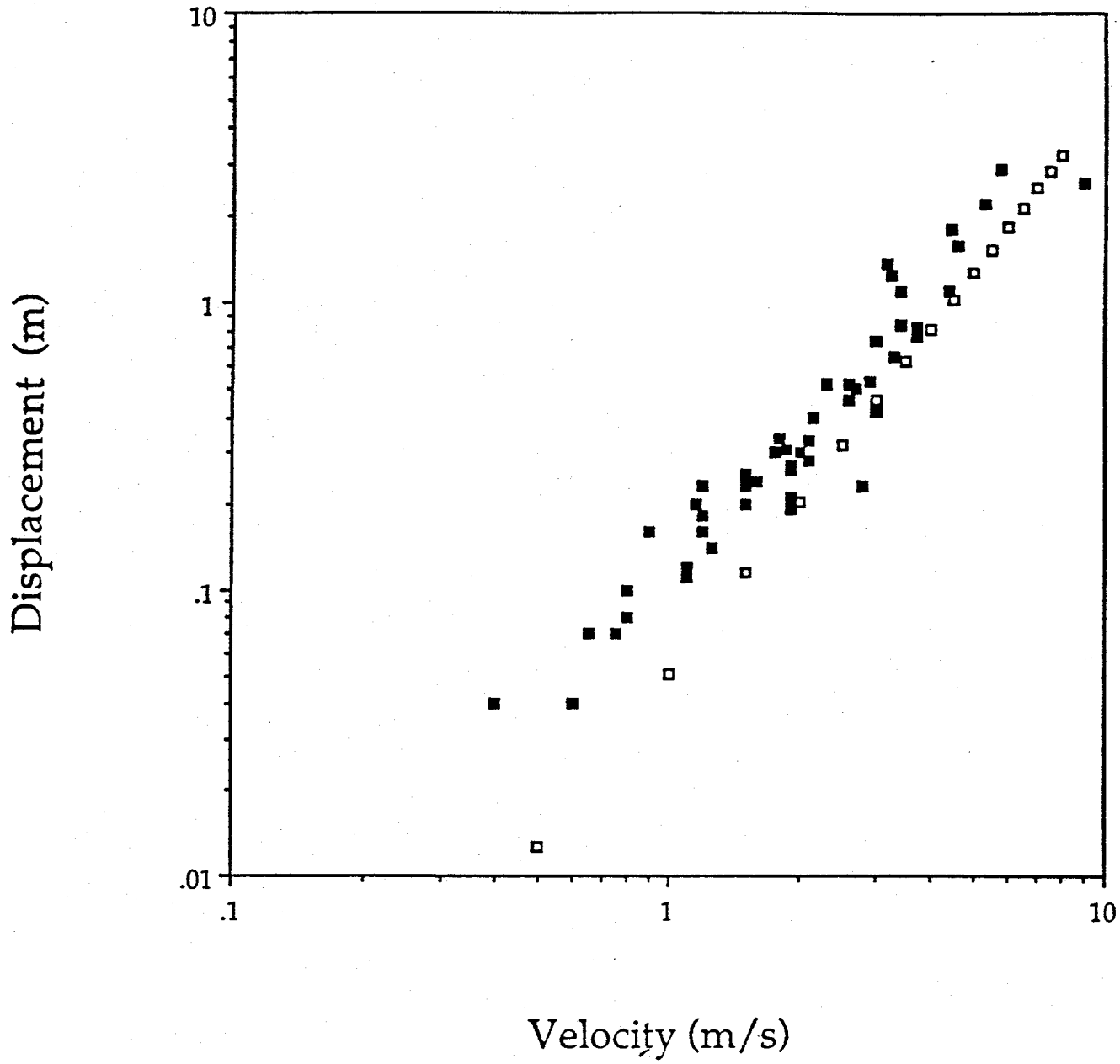

Figure 4b: Same as 4a but in logarithmic form.

Figure 5a displays the plot of displacement against dwell time along with the model (open squares). Displacements are again large for a given dwell time although the logarithmic relation (Figure 5b) does not show as large a positive bias as before. Dwell time should be linearly related to peak velocity and is displayed in Figure 6. Peak spall velocities to 2.5 m/s yield consistent dwell time estimates with divergence from the spall model at higher escape velocities representative of measurements near ground zero. This comparison of peak spall velocity and dwell time leads one to conclude that the divergence from the gravitational model observed in the velocity-displacement (Figures 4a and b) and velocity-dwell time (Figures 5a and b) comparisons must be attributed to anomalously large displacement observations.

Data show consistency with a spall tensile failure model controlled by gravitational effects although observed displacements may be as much as a factor of two to four larger than those predicted by the model. Since the displacements are estimated from the accelerations by two time integrals there is the possibility that displacement values are biased. The integration procedure has most difficulty with long periods (low signal to noise ratios) which would affect the peak displacement estimates.

A physical argument can be made to explain departure from a purely gravitational model. Spall might be a more continuous process than the simple discontinuous ballistic interpretation implies. Displacements which capture larger scale spatial effects would provide a better estimate of total spall contribution for such models. The large displacements, relative to velocities, may reflect the importance of material effects in addition to gravity in the spall model. A point measurement of velocity and displacement might not locally satisfy equations for gravitationally controlled processes as surrounding parts of the continuum continue to transmit energy in some manner. The larger displacements would imply a longer characteristic time for the spall process than that estimated by peak velocity or dwell time measurements.

PAHUTE MESA SPALL DATA

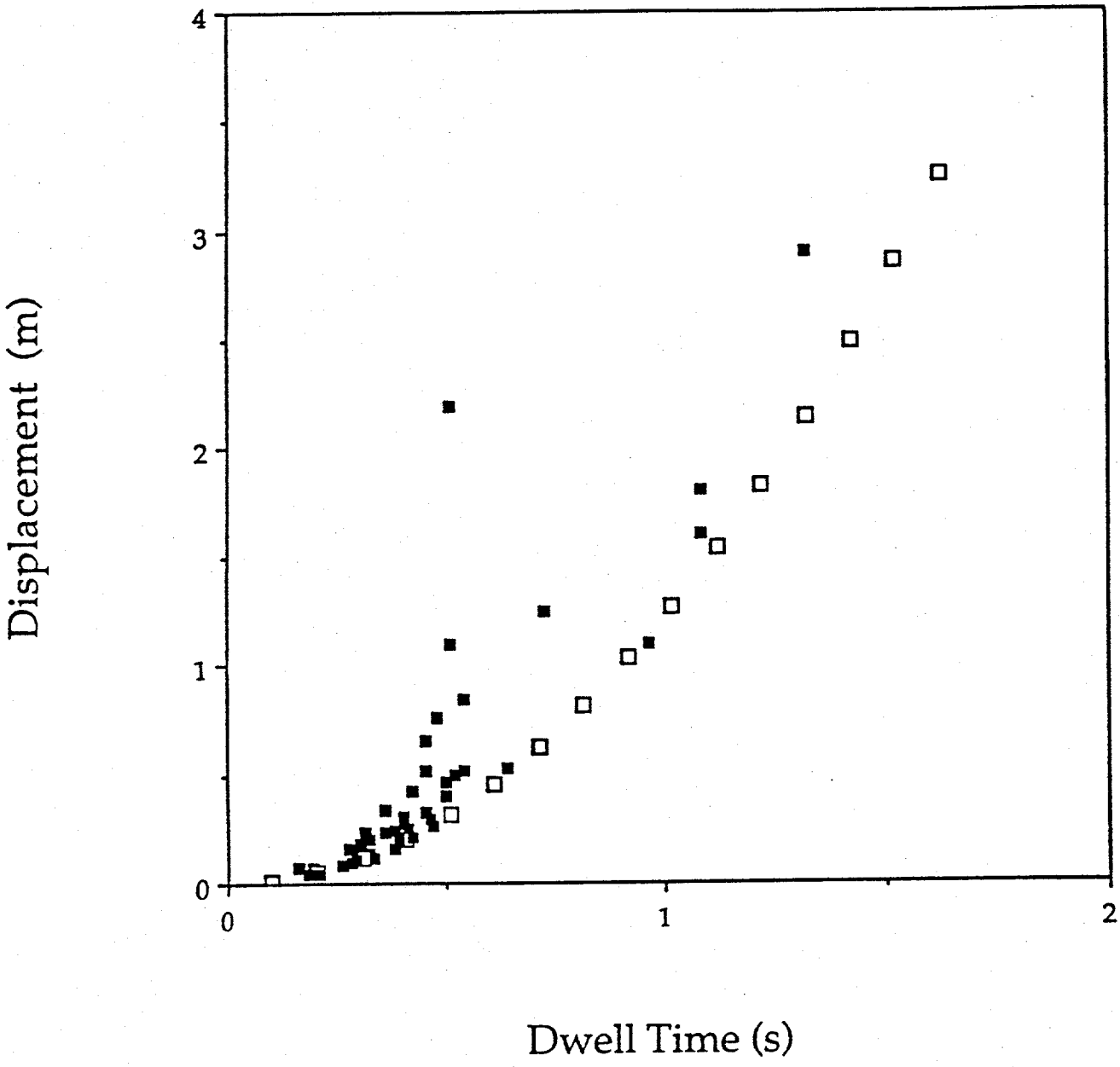

Figure 5a: Comparative plot of peak displacement and spall dwell time from nuclear explosions on Pahute Mesa. A purely gravitational spall model predicts the open squares.

PAHUTE MESA SPALL DATA

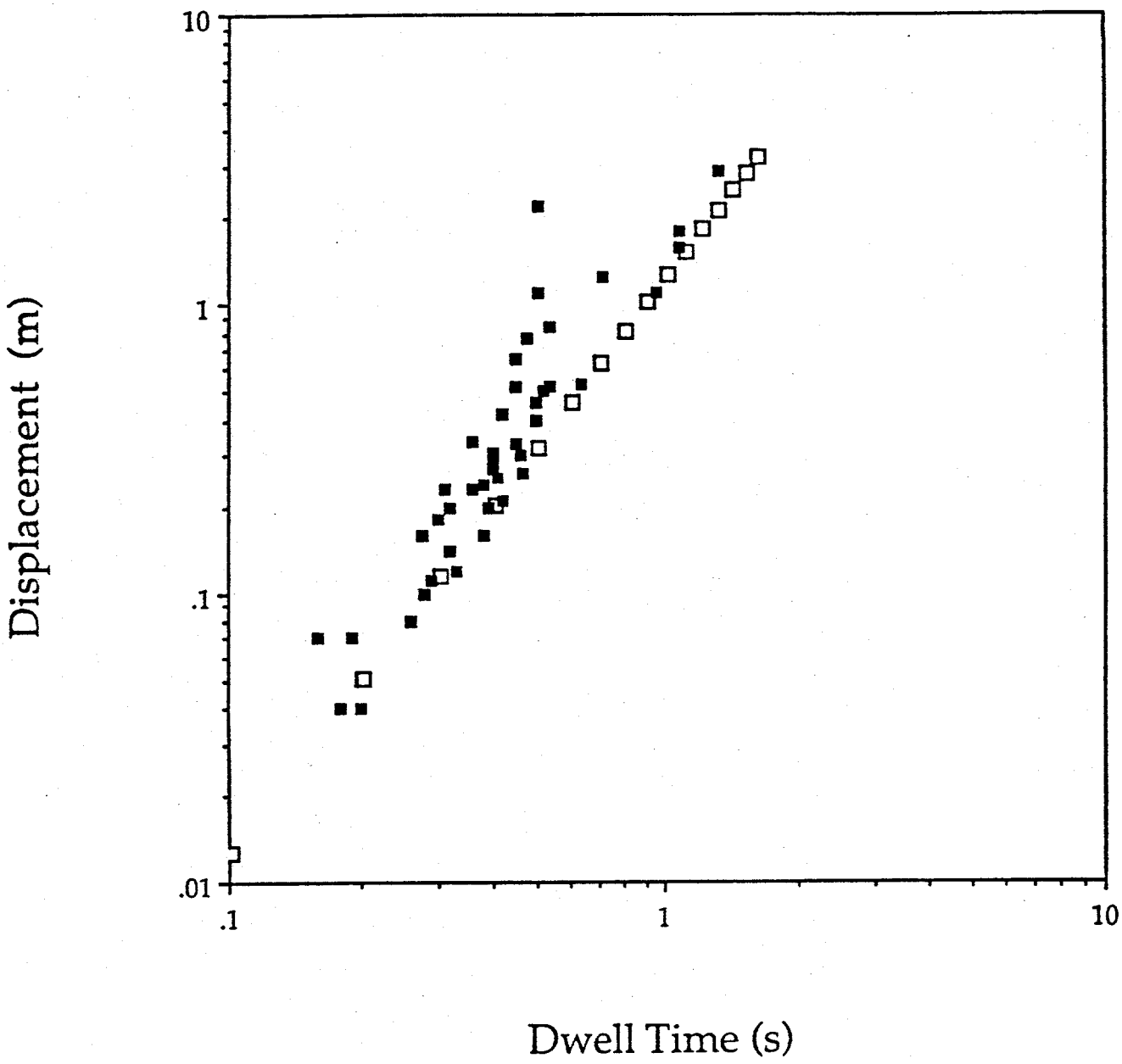

Figure 5b: Same as 5a but in logarithmic form.

PAHUTE MESA SPALL DATA

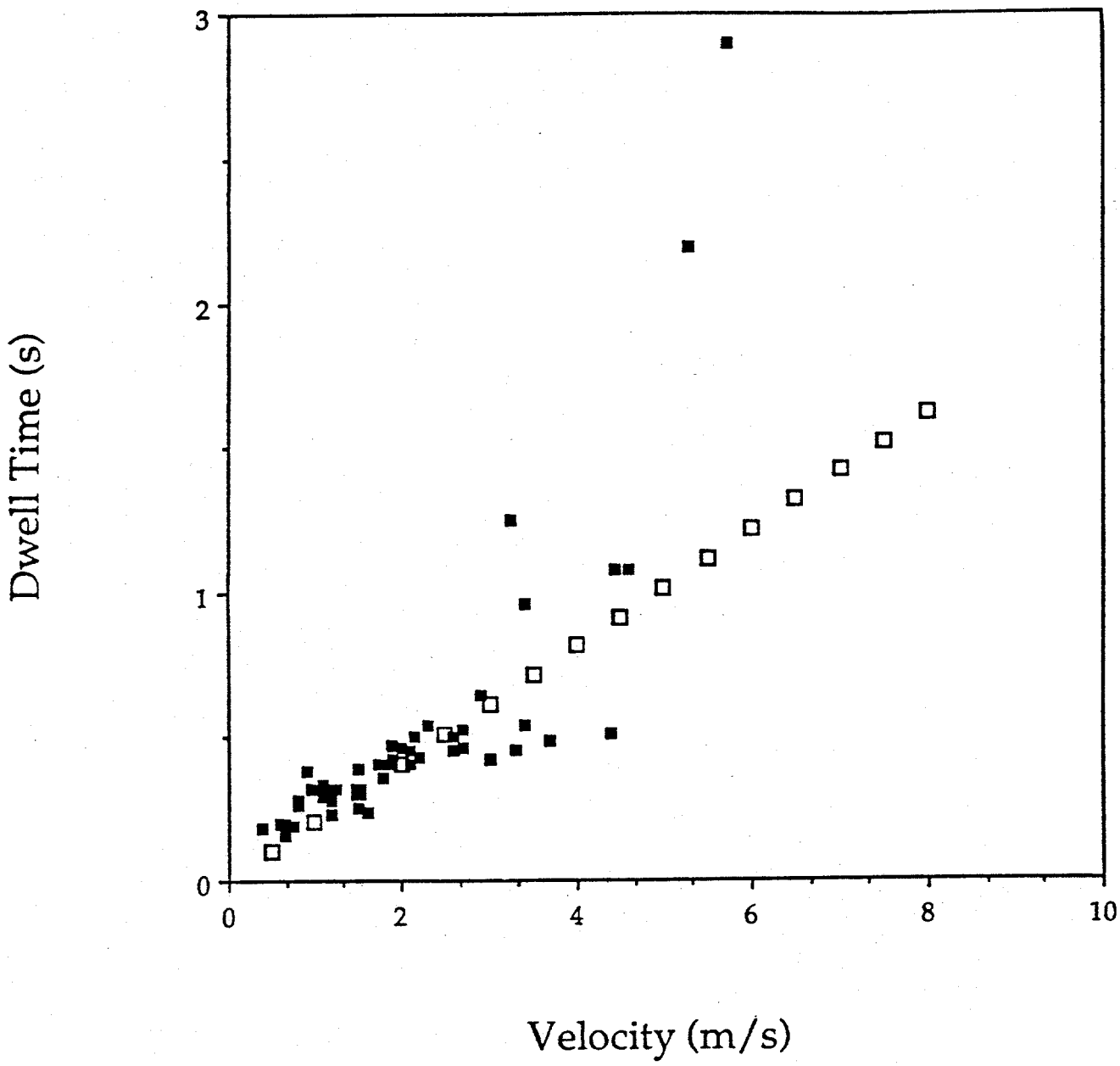

Figure 6: Comparative plot of spall dwell time and peak velocity from nuclear explosions on Pahute Mesa. A purely gravitational spall model predicts the open squares.

THEORETICAL MODELS OF DECAY

Comparison of the observational data to the decay models of various authors led to differing degrees of agreement between data and models. In order to understand the importance of a decay model on the data interpretation, a set of physical models are developed that take into account simple differences between free-field and free surface data.

MODELS, Plane wave reflection plus free field decay: A first order physical model of the spall zone ground motion is proposed that includes attenuation rates observed in the free-field coupled with a free surface interaction term which crudely accounts for incident angle of the explosion energy as it comes to the free surface and propagates back into the media. A pictorial representation of these processes is given in Figure 7a. The P ray paths for energy leaving the source are diagramed with incident angles between 10° and 60°, the U_Z (vertical) and U_R (radial) reflection coefficients are plotted as a function of range from ground zero (GZ) r, and the $1/R^2$ (R slant range) attenuation rate is also plotted against FSR.

The reflection coefficients used in these synthetics follow the work of Young and Braile (1976) and assume a planar wavefront.

$$U_R \rightarrow \frac{4\frac{\beta}{\alpha}\sqrt{1-\frac{\beta^2}{\alpha^2}\sin^2 i}}{\left(1-\frac{2\beta^2\sin^2 i}{\alpha^2}\right)^2+\frac{4\beta^3\sin^2 i\cos i}{\alpha^3}\sqrt{1-\frac{\beta^2}{\alpha^2}\sin^2 i}}$$

$$U_z \rightarrow \frac{\left(1-\frac{2\beta^2\sin^2 i}{\alpha^2}\right)2\frac{\cos i}{\sin i}}{\left(1-\frac{2\beta^2\sin^2 i}{\alpha^2}\right)^2+\frac{4\beta^3\sin^2 i\cos i}{\alpha^3}\sqrt{1-\frac{\beta^2}{\alpha^2}\sin^2 i}}$$

i : incidence angle

β : shear wave velocity

α : compressional velocity

U_Z (reflection coefficient) is plotted against FSR (r) (Figure 7b) revealing the approximate 1/r behavior where r is range from GZ. This amplitude decay is independent of any spatial decay of the wavefield in the free-field. For

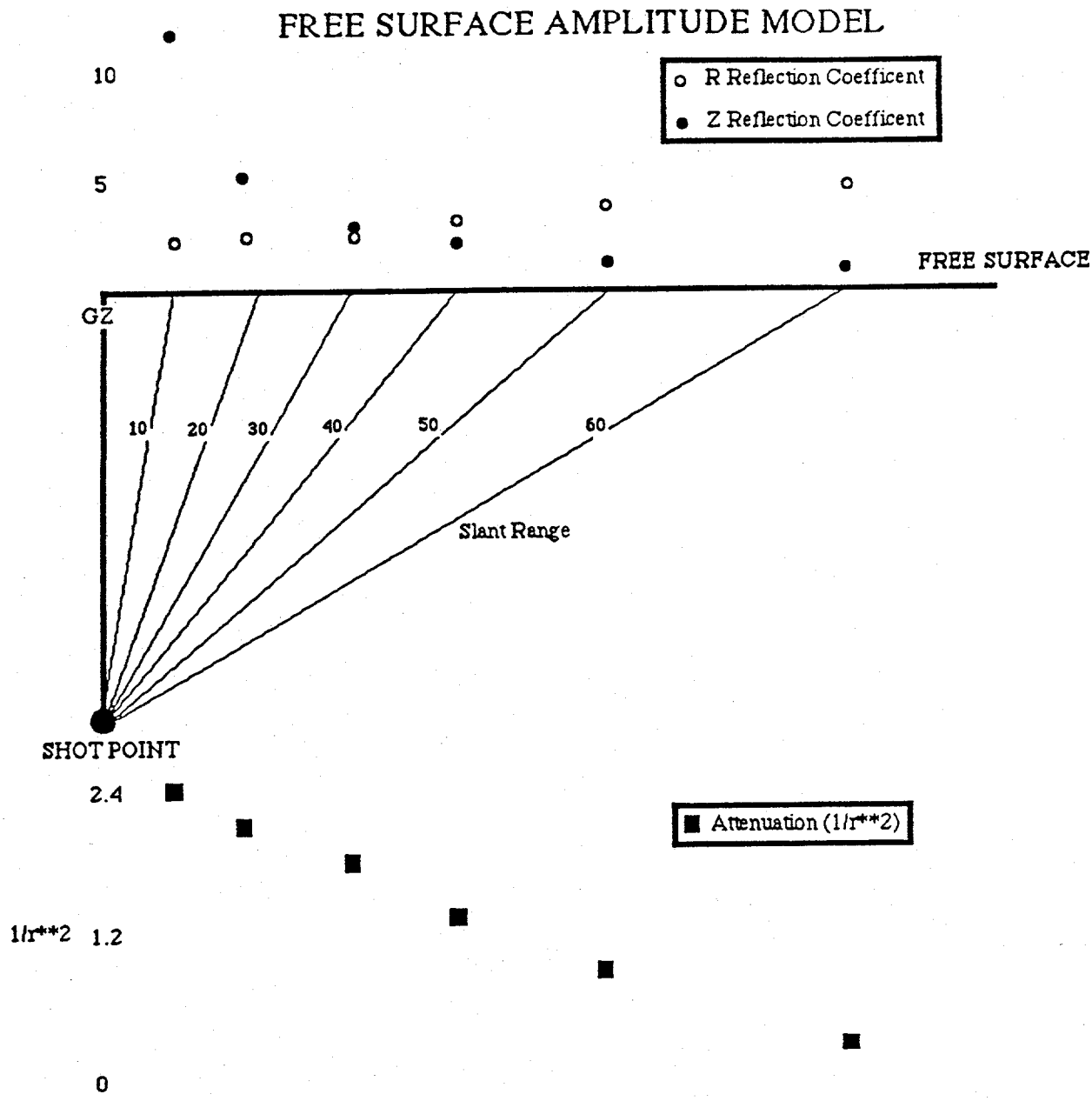

Figure 7a: Pictorial representation of the simple spall zone ground motion data that includes geometrical spreading and simple plane wave free surface interaction. The change in amplitude due to free surface interaction and geometrical spreading is given to the right of the figure.

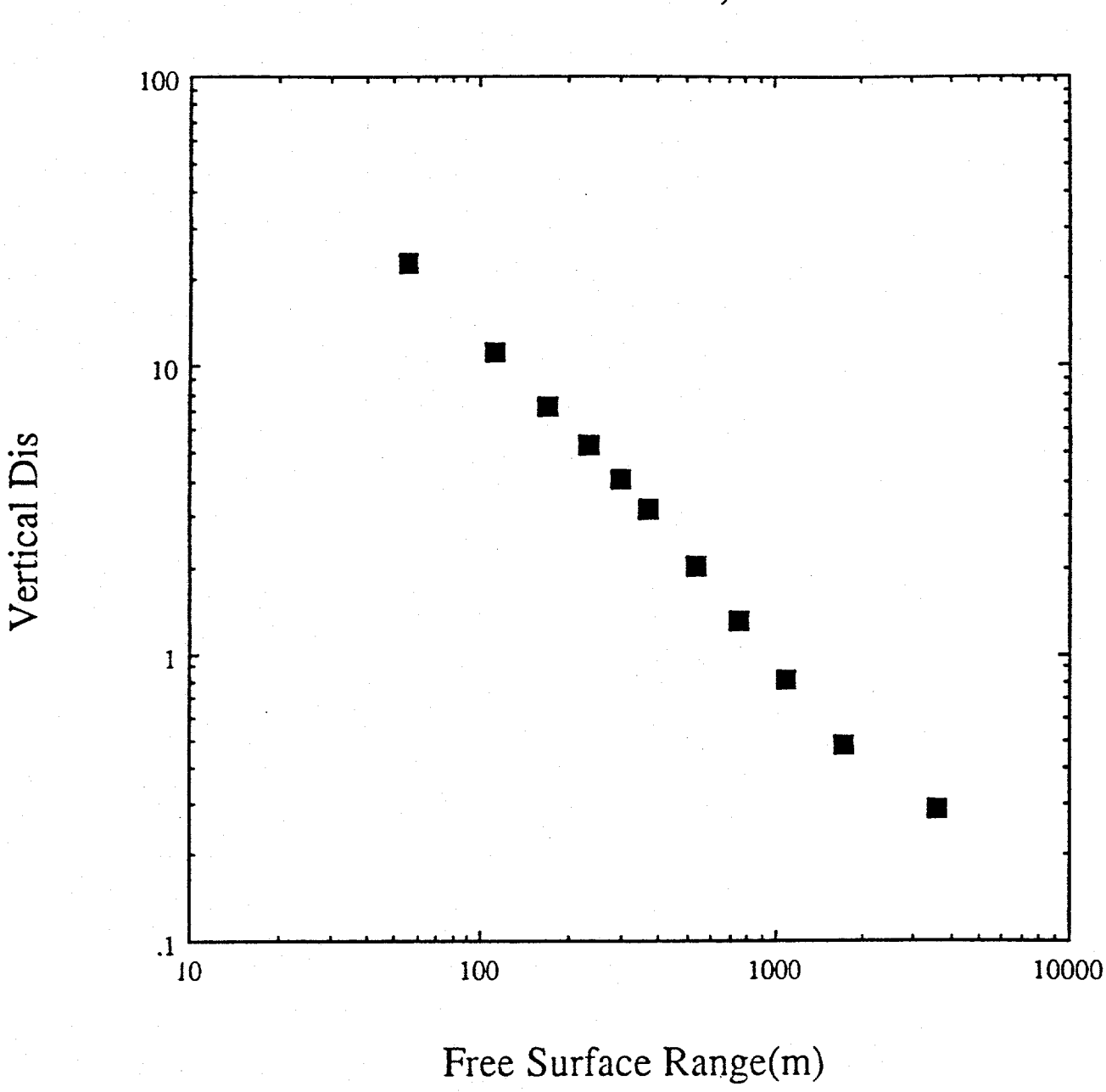

Figure 7b: Amplitude decay of the vertical motion due to the plane wave free surface reflection coefficients.

observations near GZ the total propagation path difference is small and so one might expect these free surface effect to dominate. If free-surface reflection coefficients are the dominant physical process close to GZ then a plot in the format of Figure 7b is appropriate [log (amplitude) versus log (r)]. When spatial attenuation becomes more important, then data must be plotted against SR (R). For large offsets R and r become indistinguishable.

Based on this simple discussion we propose to test the applicability of a physical model for the spall zone which includes an amplitude decay supported by the free-field data (Perret and Bass, 1975) coupled with free surface reflection coefficients. The dry tuff velocity attenuation rate from Perret and Bass is $(R/W^{1/3})^{-1.98}$ while that from Bernreuter is $(R/W^{1/3})^{-1.82}$. Simple elastic attenuation is characterized by a R^{-1} decay. Synthetics were generated with the two bounding free-field decay rates of 2 and 1. With the specified physical model a numerical exercise was designed to investigate interaction of free-field decay laws and free surface reflection effects in free surface spall data. All calculations assumed a scaled depth of 122 m. Synthetic vertical and radial data calculated to include both the free surface effect and the free-field amplitude decay were plotted in three ways in order to quantify the relative importance of the two physical processes: (1) Log amplitude vs Log R (SR, slant range) following the work of Perret and Bass which emphasizes free-field attenuation rates (Figure 8a); (2) Log amplitude vs r (FSR, free surface range) following the free surface exponential decay model (Figure 8b); and (3) Log amplitude vs Log r (Figure 8e). The first model is appropriate for a simple spatial attenuation process, the second emphasizes the free surface effects while it will be shown that the third quantifies both the free surface effect and free-field attenuation rates.

The strong effect of the free surface on synthetic data can be seen in the slant range (R) interpretation (Figure 8a). The reflection coefficient dominates amplitude decay to an approximate incident angle of 45°, i.e., to roughly one DOB horizontally (slant range 173m). For the plane wave reflection coefficient in a homogeneous half-space the radial data crosses over the vertical at a scaled slant range of 140 m and dominates at greater ranges. The combined attenuation/reflection ground motion model makes it impossible to fit a single decay law to the spall data when plotted against SSR (scaled slant range). The decay in the vertical data is overestimated and the radial data is underestimated in comparison to the free-field decay values.

For an exponential decay the log of the model data can be plotted against FSR (r) (Figure 8b) and fit with a linear slope. As in the previous representation, the fact that two physical processes (attenuation with slant range and free surface reflection coefficient) are ongoing results in the inability to explain

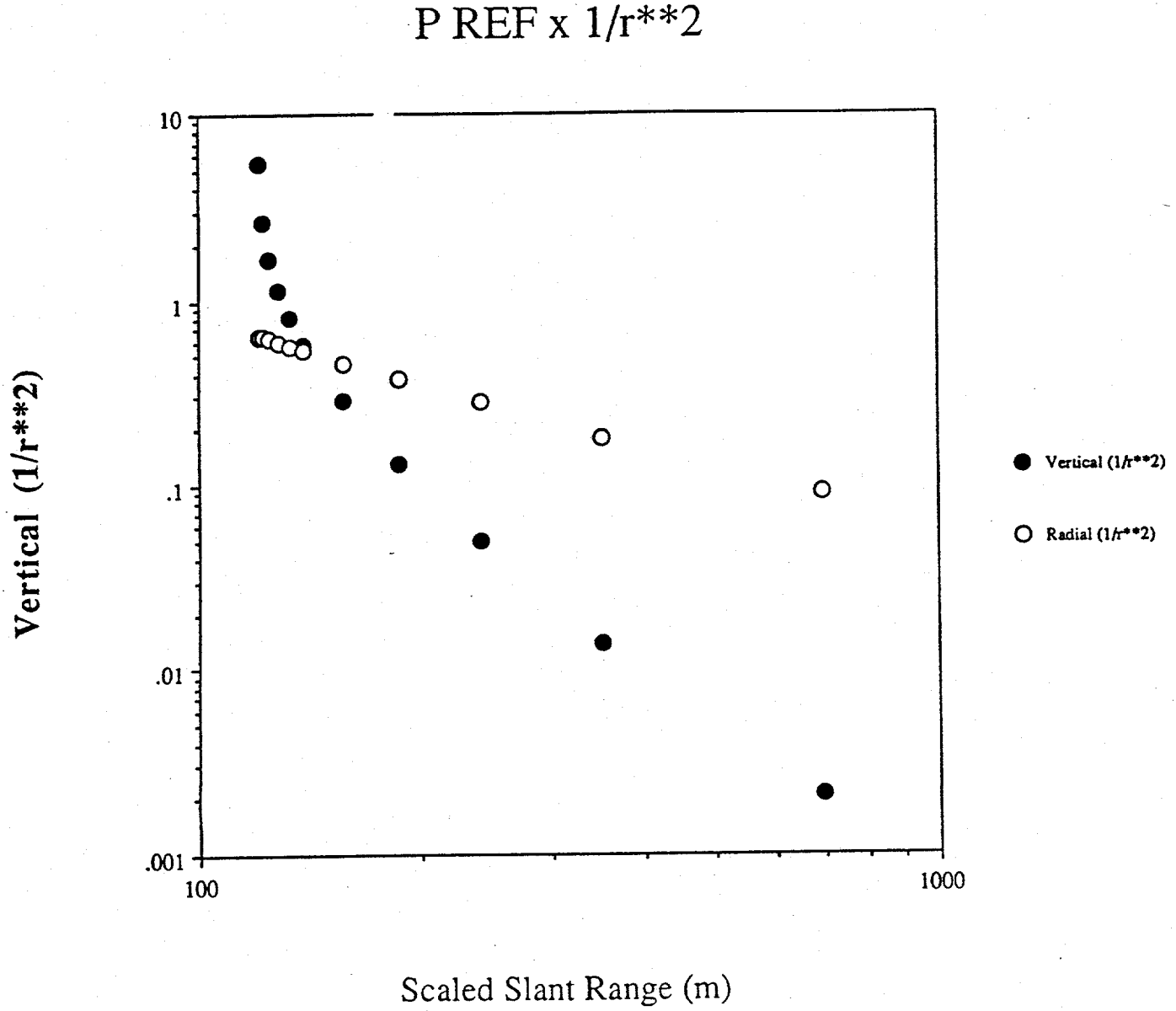

Figure 8a: Log of peak vertical velocity versus log of slant range for a synthetic model consisting of the plane wave free surface interaction and geometrical spreading of $1/R^2$.

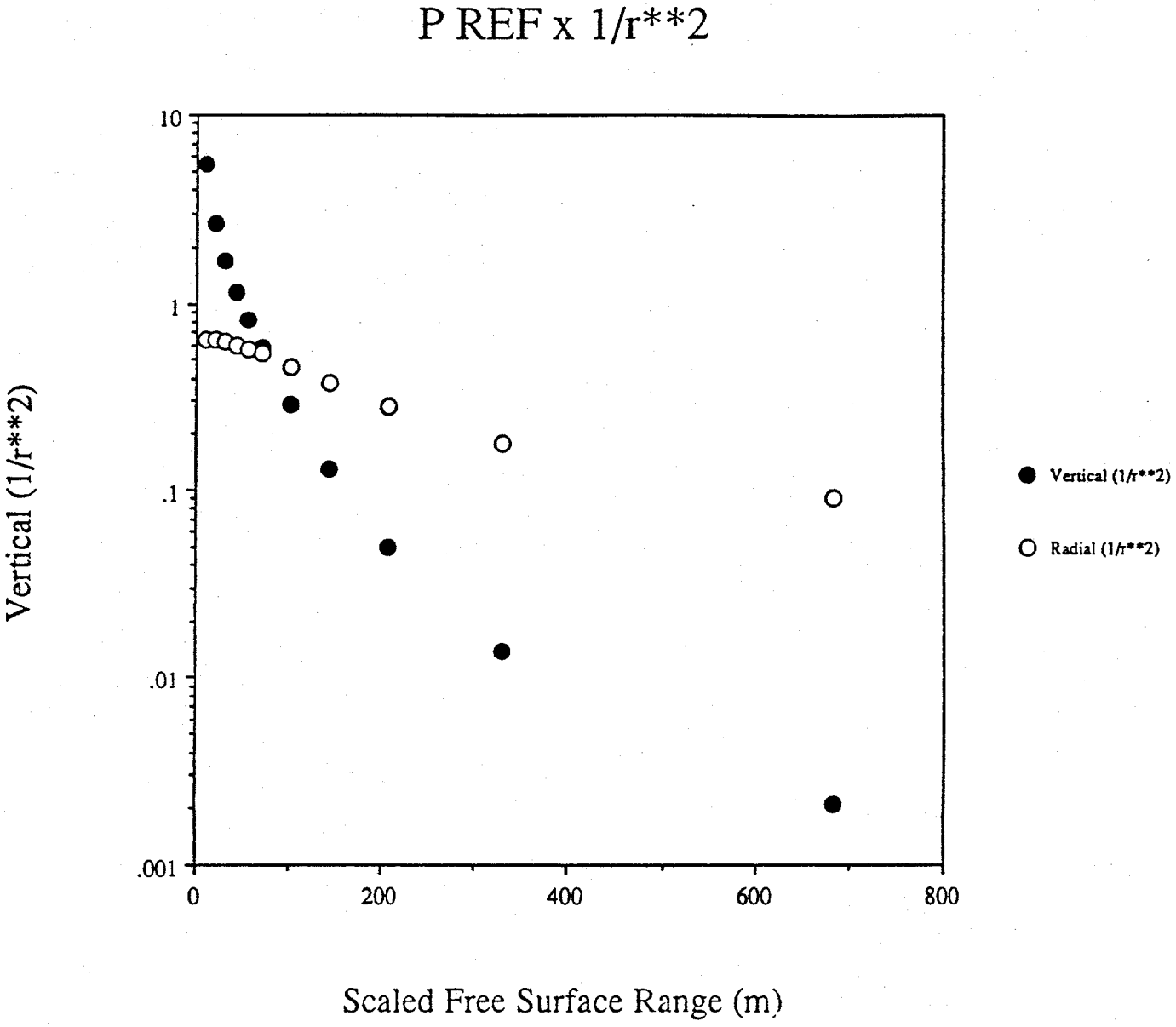

Figure 8b: Log of peak vertical velocity versus free surface range for a synthetic model consisting of the plane wave free surface interaction and geometrical spreading of $1/R^2$.

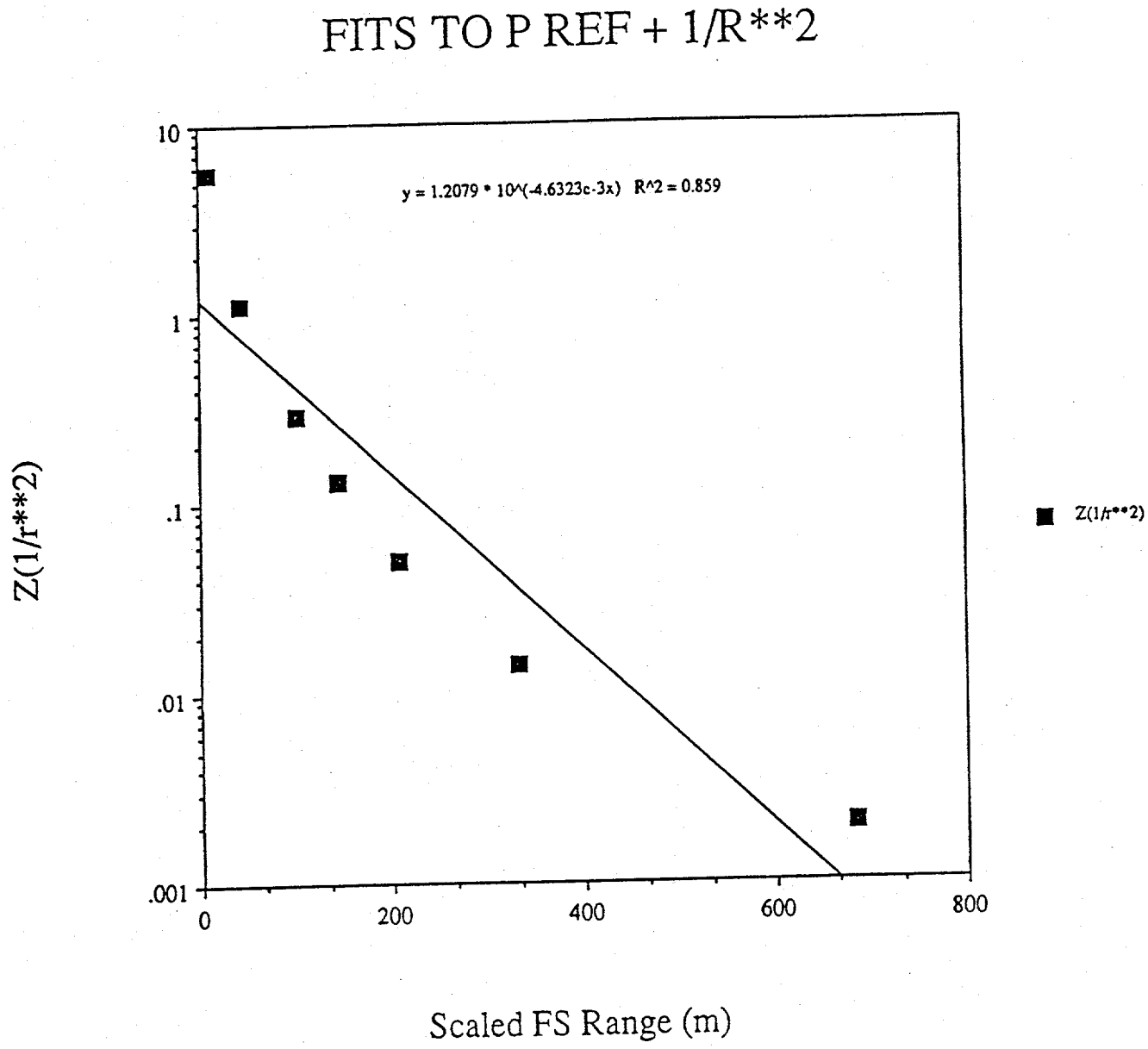

Figure 8c: Log of peak vertical velocity versus free surface range for a synthetic model consisting of the plane wave free surface interaction and geometrical spreading of $1/R^2$. Linear fits to the data are designated by the solid lines.

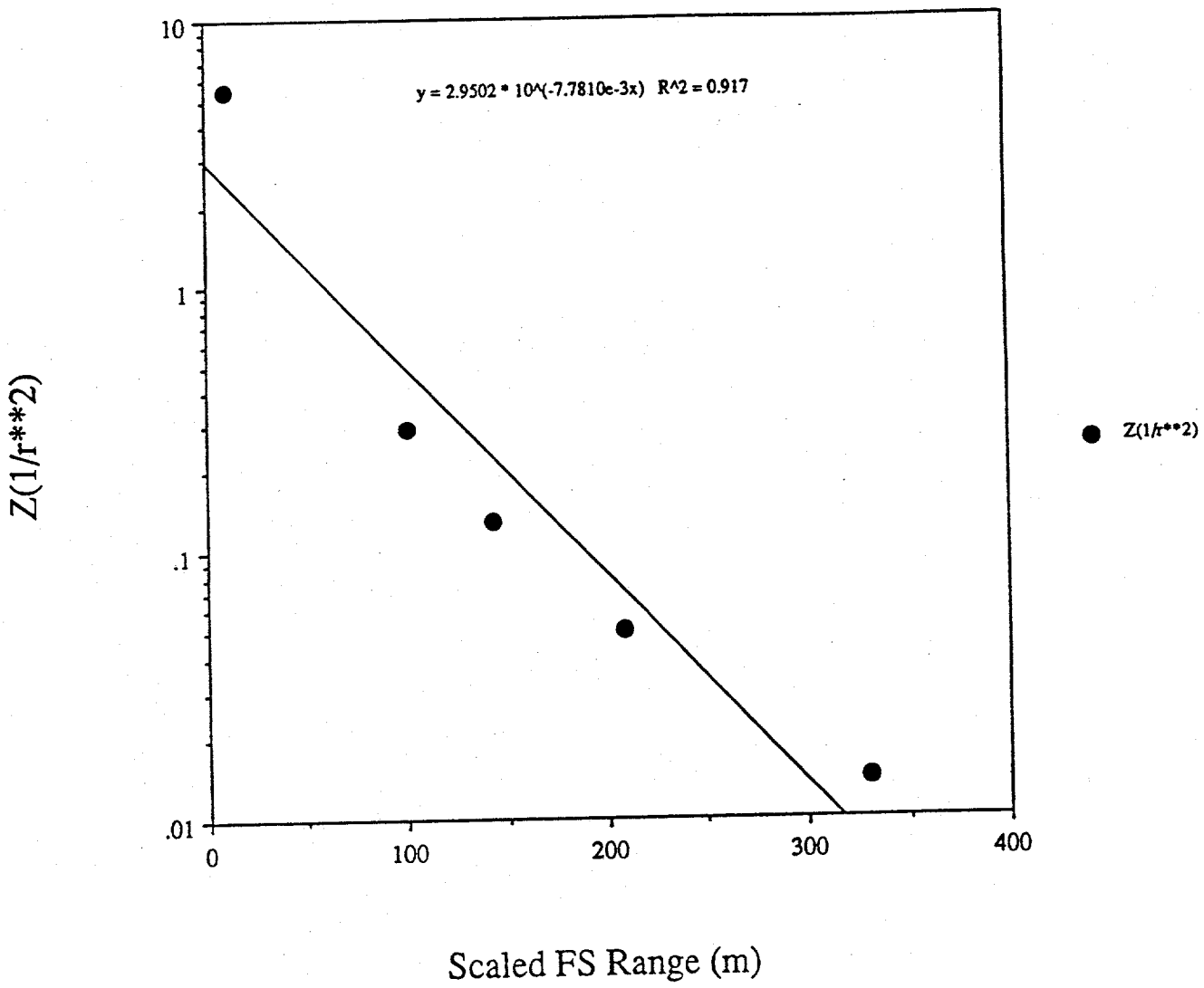

Figure 8d: Log of peak vertical velocity versus free surface range for a synthetic model consisting of the plane wave free surface interaction and geometrical spreading of $1/R^2$. Linear fits to the data are designated by the solid line.

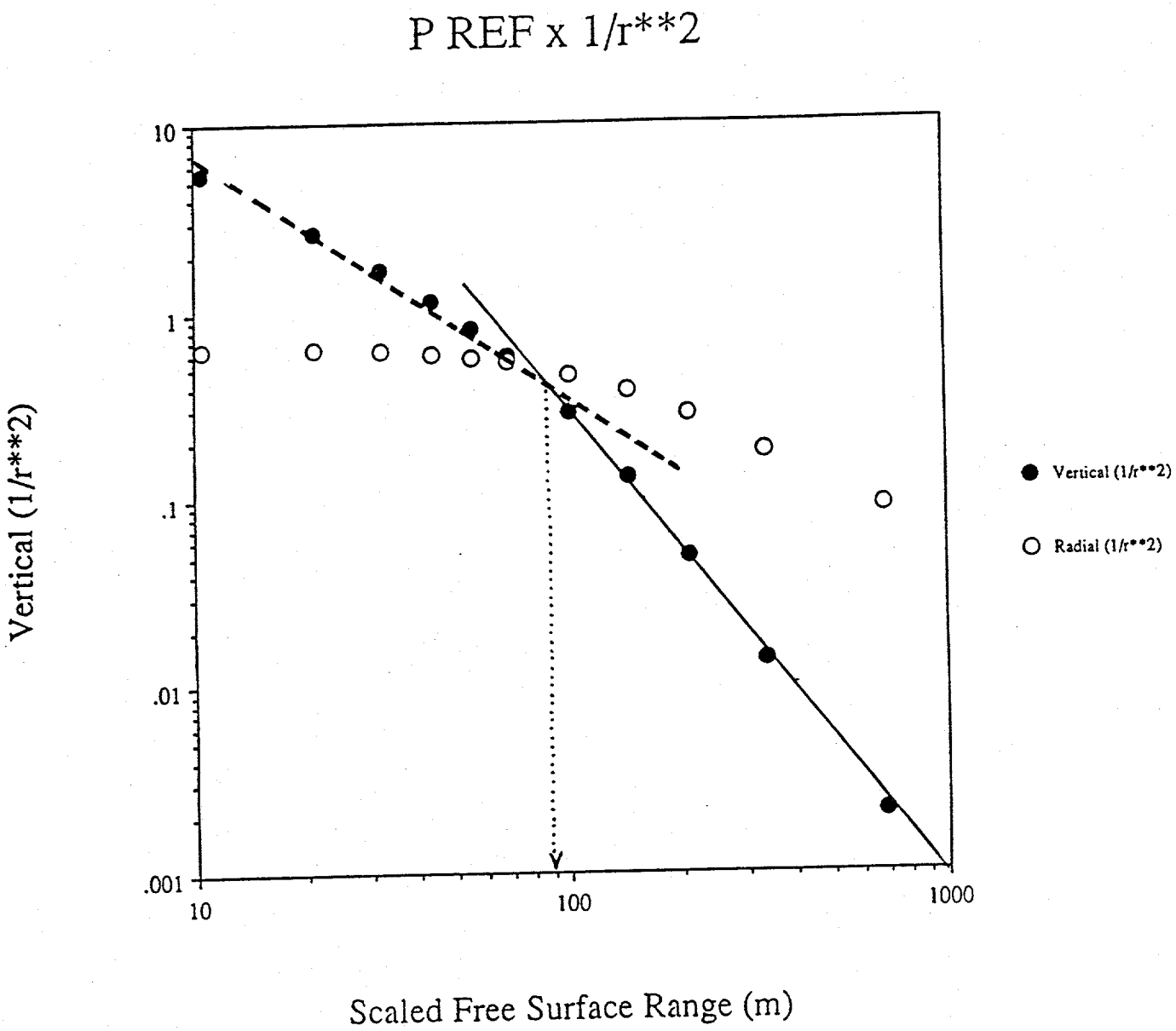

Figure 8e: Log of peak vertical velocity versus the log of the free surface range for a synthetic model consisting of the plane wave free surface interaction and geometrical spreading of $1/R^2$. The vertical data is designated by solid circles while the radial data is designated by open circles.

the data with a single decay curve. Application of the exponential model to this data leads to biased slope estimates dependent upon the free surface ranges spanned by the data and an underprediction of amplitudes near GZ where the spall velocities are the greatest. The exponential model is fit to the synthetic data to a free surface range of 700m (Figure 8c) with a decay constant of -0.0046 and to a range of 360m (Figure 8d) with a decay constant of -0.0078. Both fits under predict data at the closest ranges.

The final data representation plots the log of amplitude versus the log of FSR (r) (figure 8e). The reflection coefficient results behave as $r^{-1.26}$ for the vertical synthetics close to GZ (Figure 7b). As range increases, the difference between SR and FSR decrease resulting in linear decay law representative of attenuation with propagation distance. The interpretation of the vertical synthetic peaks in Figure 8e is in terms of a moderate decay ($r^{-1.26}$) between GZ and a scaled free surface range (SFSR) of 70-100 m, followed by the more rapid decay ($r^{-2.5}$) beyond 100 m representative of the material properties. The radial data in contrast displays little amplitude variation to 70-100 m followed by a slow decay (r^{-1}) at greater ranges thus rising in amplitude relative to the vertical component. This final representation would argue that the spall ground motion data taken at the free surface should be interpreted in terms of two decays with surface range, one dominated by the free surface and the other by the material properties.

MODELS, Reflectivity synthetics: The initial set of synthetics were quite simple but allowed the investigation of interactions between free-field and free surface effects and the geometry of the problem. The next step in complexity is inclusion of spherical wave propagation effects in layered materials. Although this representation is still linear, it allows an assessment of these additional wave propagation phenomena. This representation also allows the inclusion of source time function and strength. Full wave synthetics using the modified reflectivity methodology (Muller, 1985) were computed as a check against the simple plane wave reflection models. This methodology accounts for the complete response of plane layered structures and includes both body and surface waves. Conversions at interfaces are included as well as the spherical nature of the wavefront. Range effects introduced by anelasticity are included. Unlike the simple reflection coefficient synthetics, no free-field decay rate is assumed.

The velocity model (HOLE) used in the calculation of these full wave synthetics is given in Figure 9a. The source was at a depth of 616 m which is close to the scaled depth for a 150 kt explosion. The velocity model was taken to be characteristic of a Pahute Mesa structure. Vertical and radial velocity waveforms between 0.1 and 3.0 km (FSR) are given in Figure 9b. Waveforms

PAHUTE MESA P VELOCITY MODELS

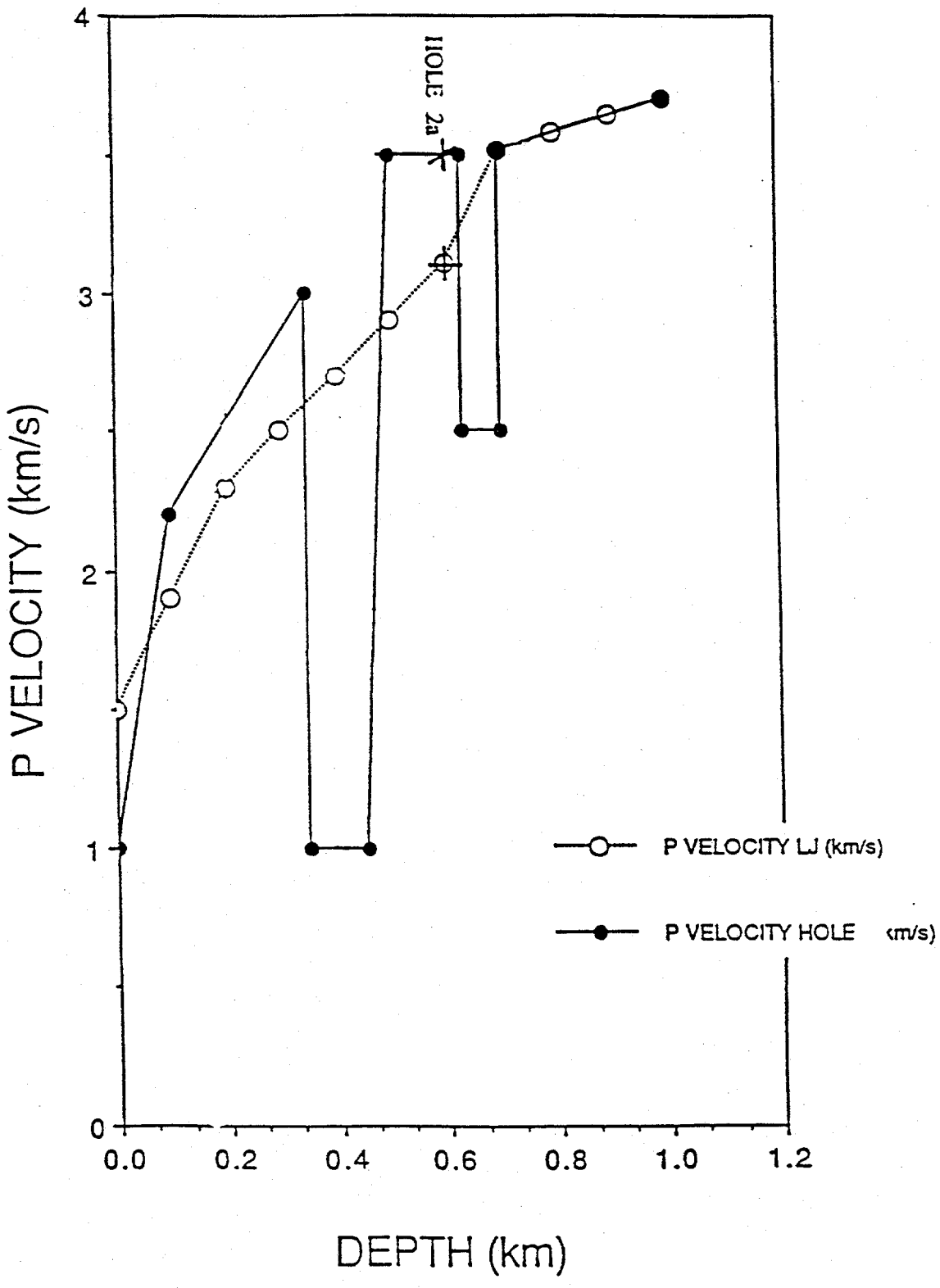

Figure 9a: Representative Pahute Mesa P velocity model (solid line) used to calculate synthetic seismograms for this study. Source depth is designated as HOLE 2a.

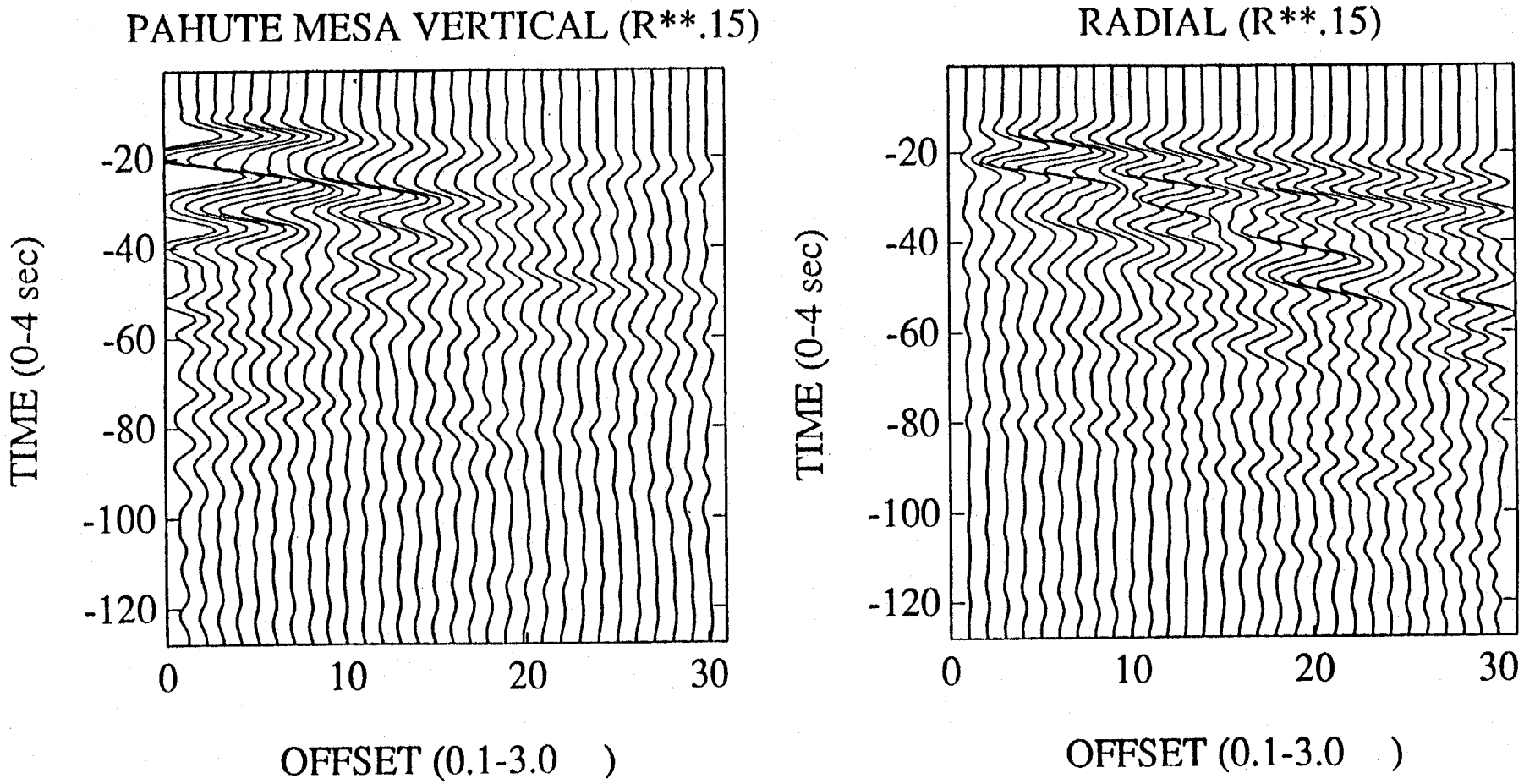

Figure 9b: Vertical and radial reflectivity velocity seismograms for the velocity model in Figure 9a. Seismograms are generated for free surface ranges of 0.1 to 3.0 km at 0.1 km increments.

have been multiplied by $r^{0.15}$ to account for the slight decay of the wavefield directly above the explosion. Vertical waveforms show little decay to 600-700m in this plot. Velocities decay much more rapidly beyond this FSR. For a 150 kt shot this transition region corresponds to a SFSR of 113-132 m. . Peak vertical velocity as a function of free surface range is reproduced in Figure 9c. The least squares fit to the amplitude decay to a SFSR (100m/ $kt^{1/3}$) was $r^{-0.15}$ while the decay rate beyond this range was $r^{-1.30}$. This model predicts little decay in peak vertical velocities out to a scaled free surface range of 100 $m/kt^{1/3}$. Since this region is the one in which spall depth is the greatest, these synthetics would suggest that this region would dominate spall momentum estimates.

The radial synthetic data in contrast to the vertical increase in amplitude away for ground zero reaching amplitudes comparable to the vertical at a FSR of 600 m and then decay at a rate similar to the vertical synthetics (Figure 9d). The layered media and spherical nature of the wavefront account for the differences between this model and that from earlier synthetics. Reflectivity synthetics which include the effects of all conversions at the free surface and the spherical character of the wavefront predict much less focusing of amplitudes near GZ in comparison to the plane wave model. Radial motions merge with the vertical data at a scaled range near 100 m but do not significantly rise above the vertical data as in the simple reflection coefficient model.

The two synthetic models support a dominance of vertical ground motion out to a FSR of approximately 1 DOB followed by a rapid decay of motions beyond. This characterization may be responsible for the confinement of the spall zone to FSR which are near 2 -3 DOB. One might expect significant variability in the spall zone in the FSR of 1-3 DOB because it is in this region that motion levels are decaying most rapidly. Spall contributions in the FSR extending to 1 DOB may be less variable based on the consistency of peak vertical motions from the synthetics.

One of the purposes of this synthetic study was to assess the importance of decay model in fitting free surface synthetics. Two additional models, exponential in FSR and power law in SR were fit to the data. Figure 9e displays the fit of the exponential model to the reflectivity peak velocities. The fit underestimates the synthetics closest to GZ out to a FSR of 1 DOB. The decay constant in this fit is 0.93.

The SR interpretation of the synthetic data is given in Figure 9f. A single decay constant of -1.65 matches the data although there are subtle mismatches for velocities close to GZ. This second representation of the data is a viable option to FSR plots. It does not emphasize the spall zone data which is the primary

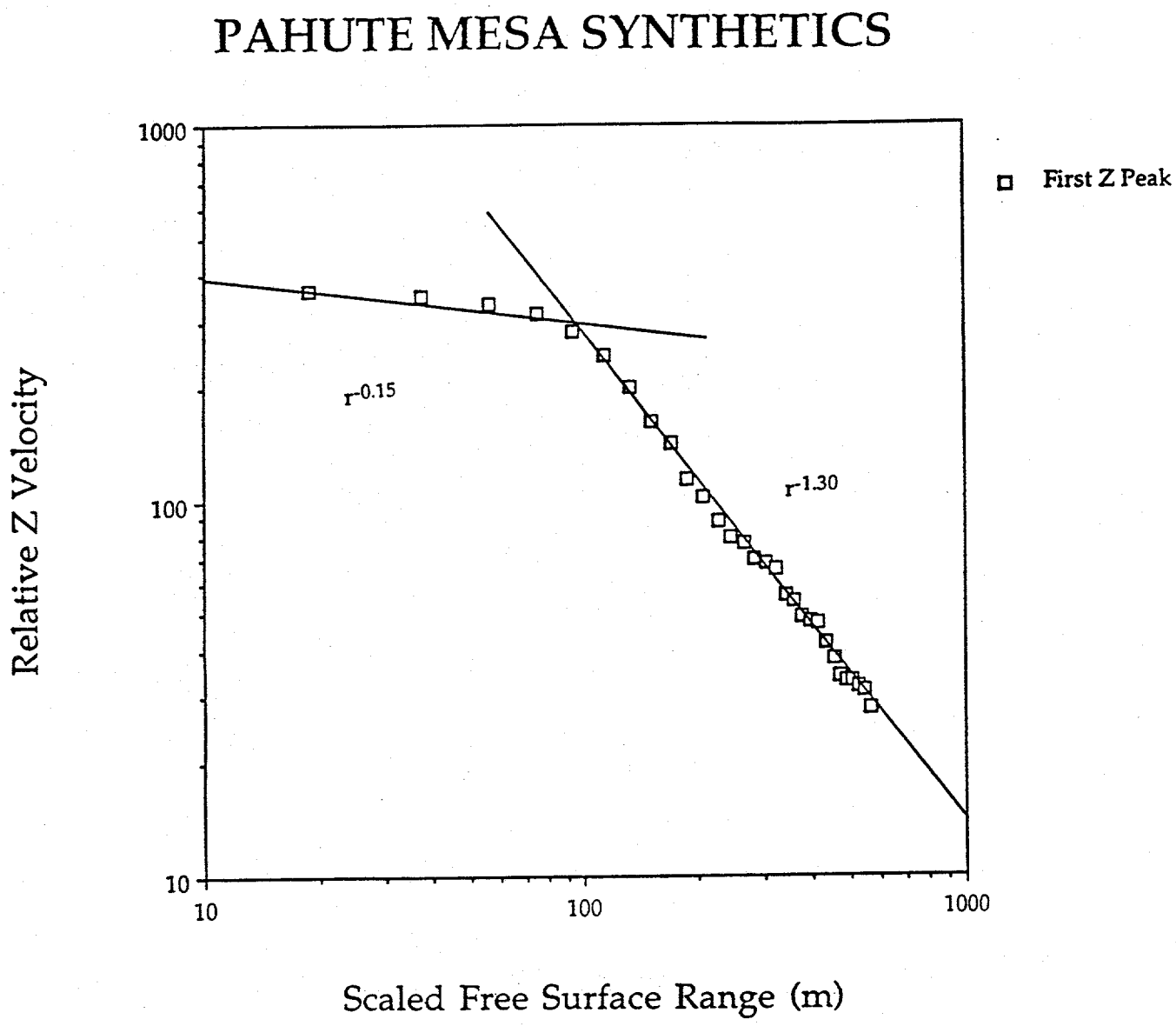

Figure 9c: The log of the peak vertical velocities from the synthetic seismograms in Figure 9b plotted against the log of the free surface range. Experimentally determined decay curves for data at ranges less than and greater than 100 $m/kt^{1/3}$ are given.

HOLEX REFECTIVITY SYNTHETICS

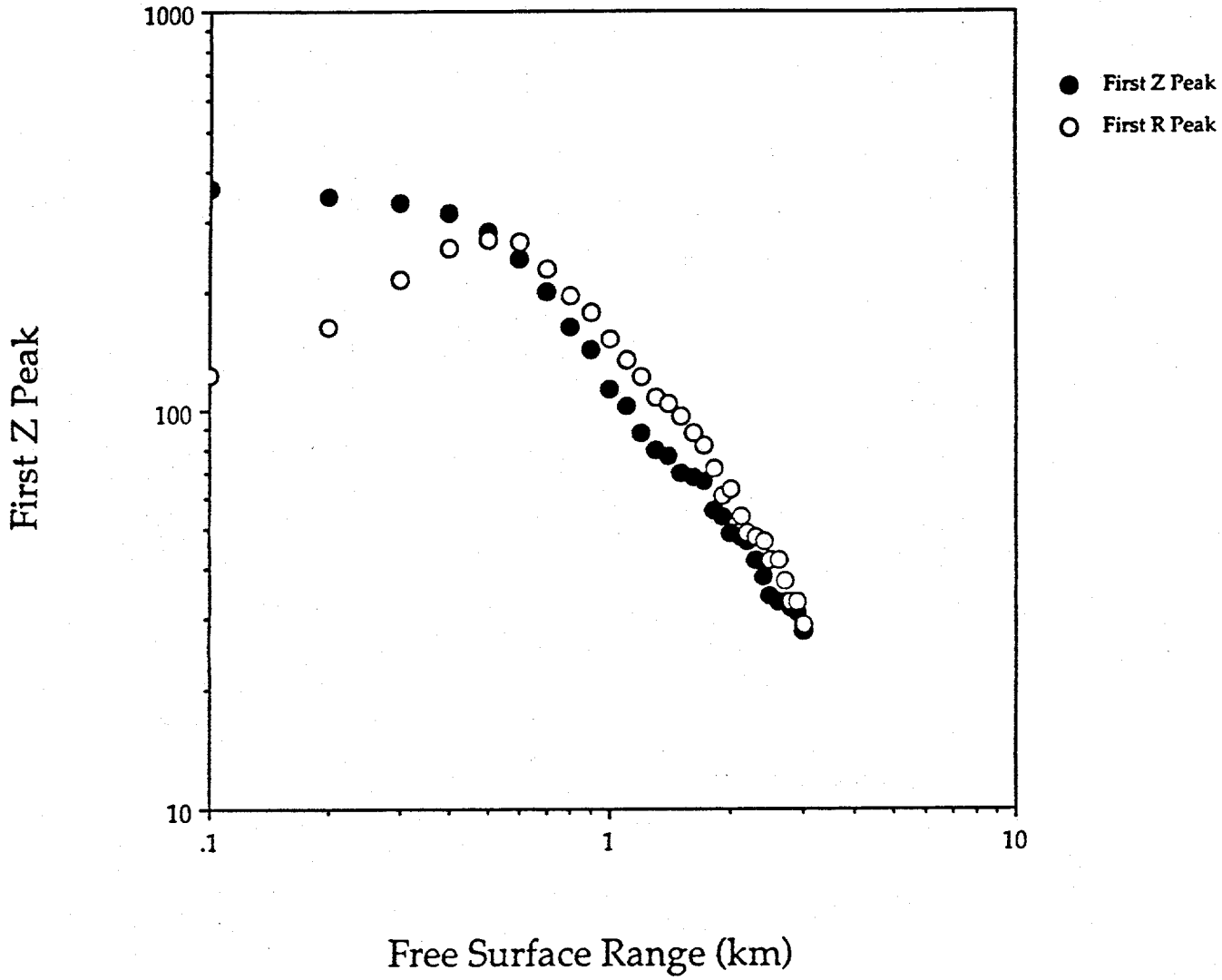

Figure 9d: The log of relative vertical (solid circles) and radial (open circles) peak velocities from Figure 9b plotted against the log of free surface range.

Pahute Mesa Synthetics

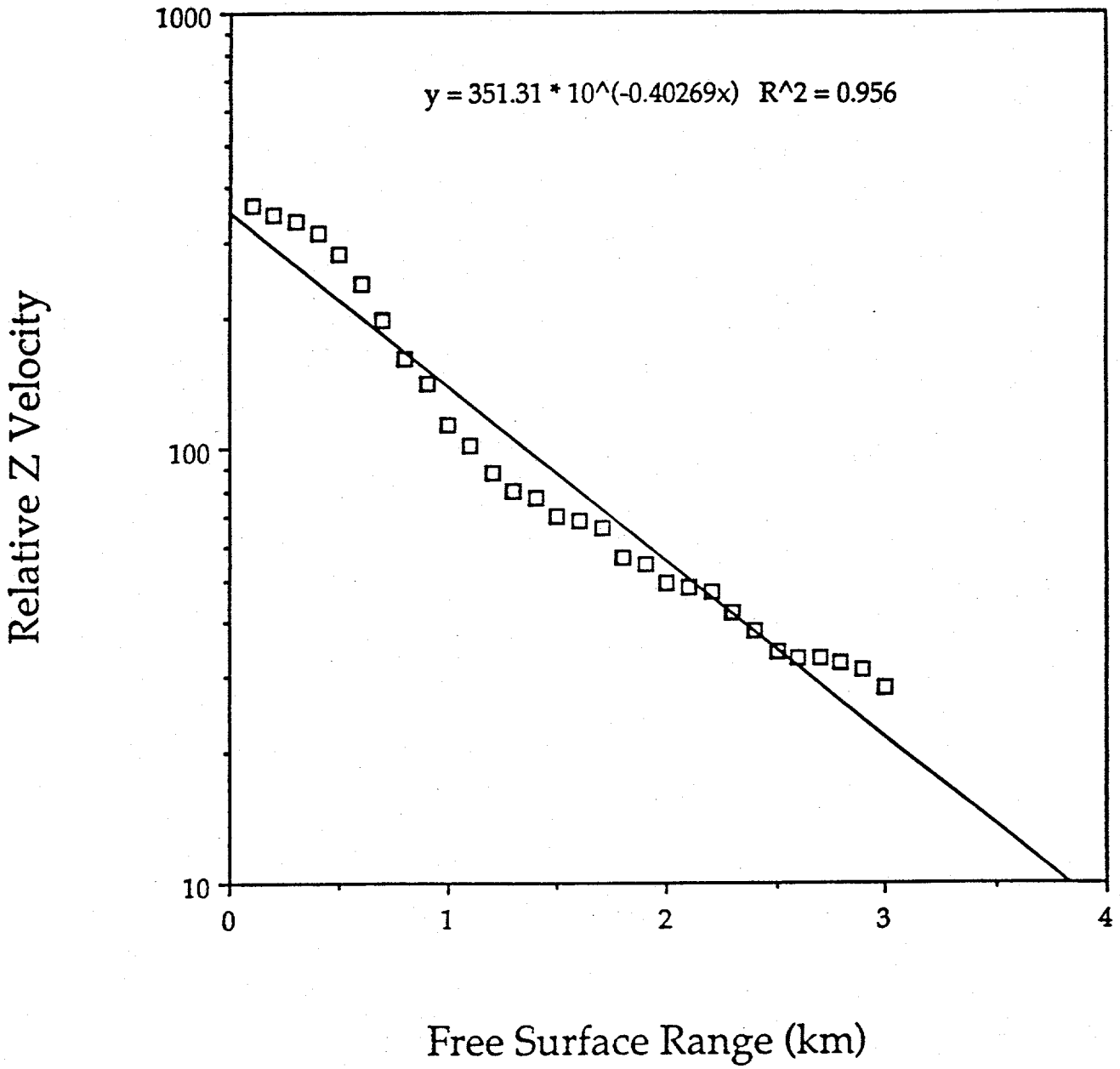

Figure 9e: The log of peak vertical velocity from synthetic data in Figure 9b plotted against free surface range. An exponential model has been fit to the data.

Pahute Mesa Synthetics

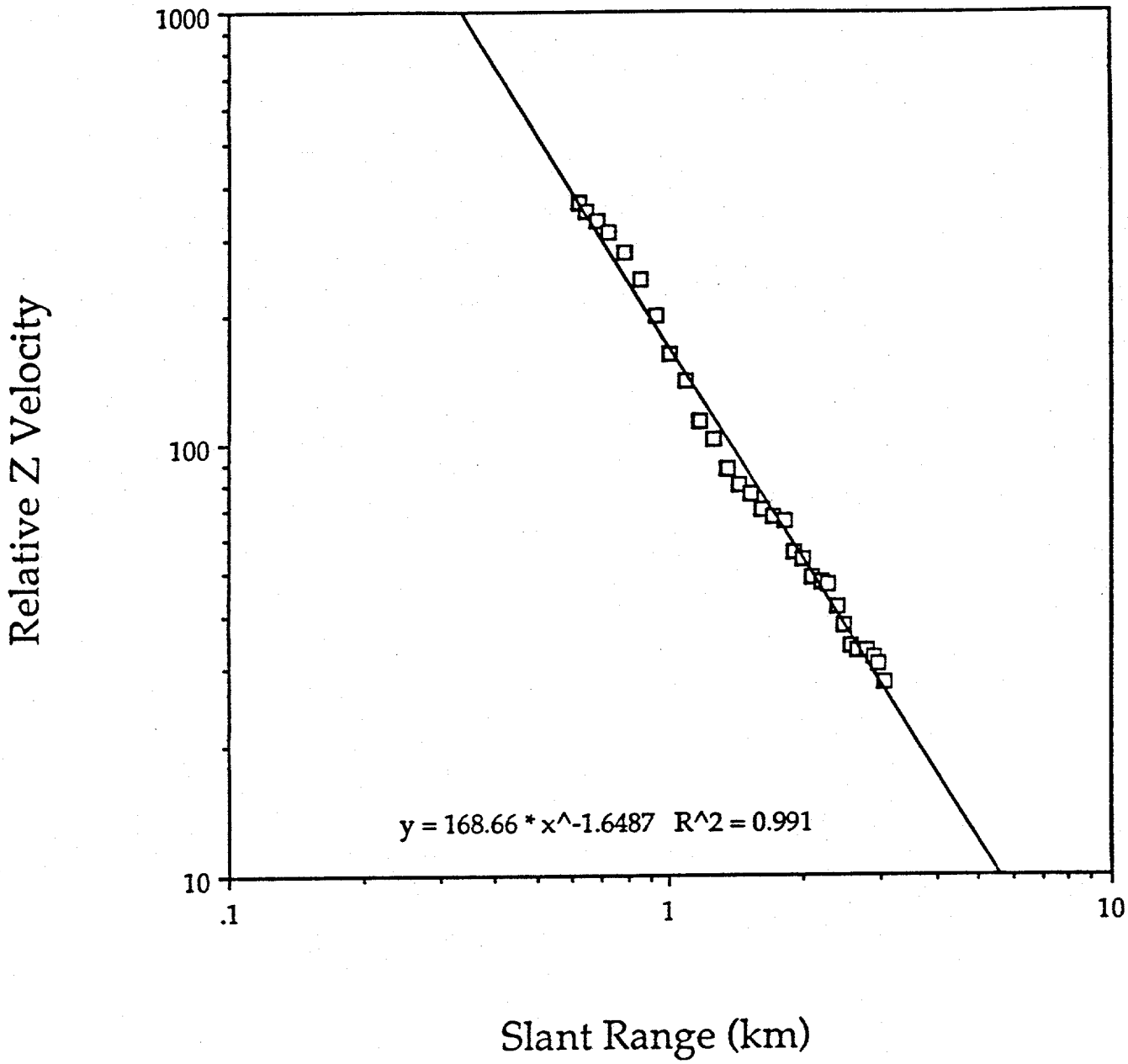

Figure 9f: The log of peak vertical velocity from the synthetic data in Figure 9b plotted against the log slant range. A power law model has been fit to the data.

concern of this work. The different decay models fit to the synthetics are summarized in Table 2. The range of decay constants (-0.15 to -1.65) illustrate the importance of geometry in the interpretation of the spall zone data. Care must be taken in comparing decay constants determined by different authors because of these geometrical effects.

Table 2: Velocity Decay Laws from Data

Model Type	**Decay**
Power law, slant range	$R^{-1.65}$
Power law, free surface range	
(0-100m/kt$^{1/3}$)	$r^{-0.15}$
(100-500m/kt$^{1/3}$)	$r^{-1.30}$
Exponential, free surface range	$e^{-0.93r}$

MODEL AND DATA COMPARISONS

Predictions of the decay models can be compared to the observational data. The log of the motion data (Figure 3) is replotted against the log of SFSR (scaled free surface range) (Figure 10) in order to emphasize the data within the spall zone (0-244 $m/kt^{1/3}$) These representations illustrates how little data are available between GZ and a SFSR equal to 60-100$m/kt^{1/3}$, the range in which both synthetic models predict the greatest spall zone motions. The data are consistent with two decay curves, one of moderate slope between GZ and 70-100 $m/kt^{1/3}$ followed by the more steeply sloping curve beyond representative of the material attenuation rate.

Radial data can also be compared to vertical data for model validation (Figure 11). Vertical motions are greater than radials to a range just beyond 100 $m/kt^{1/3}$. Radial data merge with the vertical at this range. Unlike the reflection coefficient synthetics, but in agreement with the reflectivity synthetics, the radial data do not rise significantly above the vertical at greater ranges. The velocity gradient in the near surface layers turns the waves to the vertical with increasing free surface range thus tending to equilibrate the vertical and radial motions in the reflectivity synthetics.

The observational data are in apparent agreement with the simple two process physical model for the free surface spall data. The velocity data from 0-100 $m/kt^{1/3}$ has a decay of $r^{-0.13}$ while the reflectivity synthetics decay as $r^{-0.15}$. Beyond 100 $m/kt^{1/3}$ the data decay as $r^{-1.22}$ while the synthetics decay as $r^{-1.30}$.

Although the fits of the exponential and SSR (scaled slant range) models to the synthetics were not as good near GZ, these model fits can also be compared to similar fits to the observational data. The velocity data were fit with the exponential model in Figure 12. The decay constant was -0.003. The majority of data near GZ are underestimated. The SSR fit to the velocity data is given in Figure 13. The velocity data has a decay constant of -1.88 while the synthetics (Figure 9f) gave a value of -1.65. SSR decay constants are greater than the values determined when the data was interpreted in terms of SFSR (data: -1.22 to -1.88; synthetics: -1.30 to -1.65). These comparisons show bias which can be introduced depending on the assumed decay model.

The conclusion drawn is that for routine underground nuclear events at NTS, free surface motions change little to a SFSR near $100m/kt^{1/3}$ followed by an increased decay with range. Plotting the log of the amplitude measurement against log (r-SFSR) is the best display for separating these effects. At close

Pahute Mesa Spall Data

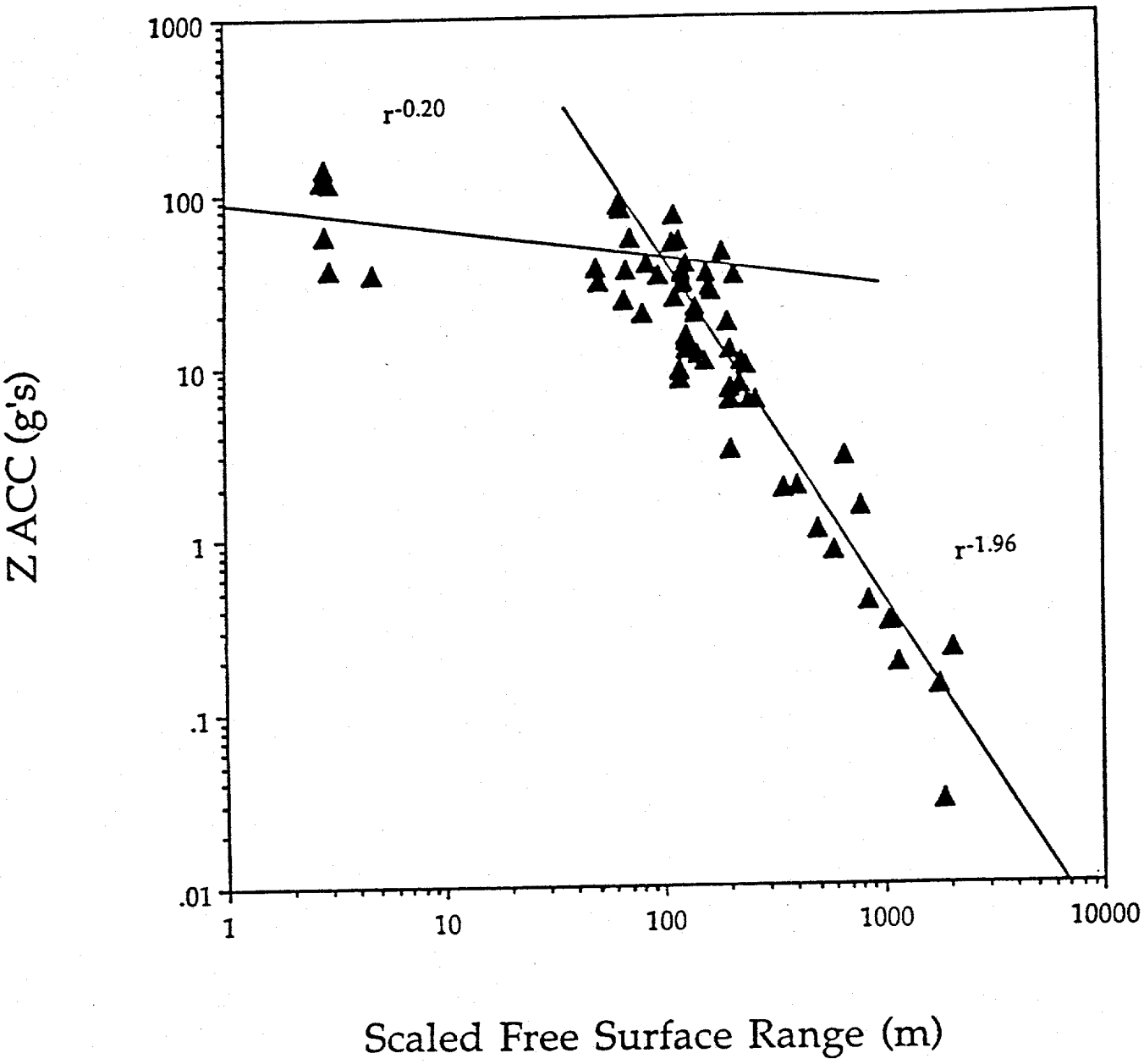

Figure 10a: The log of scaled peak acceleration versus the log of scaled free surface range for Pahute Mesa data. Power law models were fit to the data for ranges less than and greater than 100 $m/kt^{1/3}$.

Pahute Mesa Spall Data

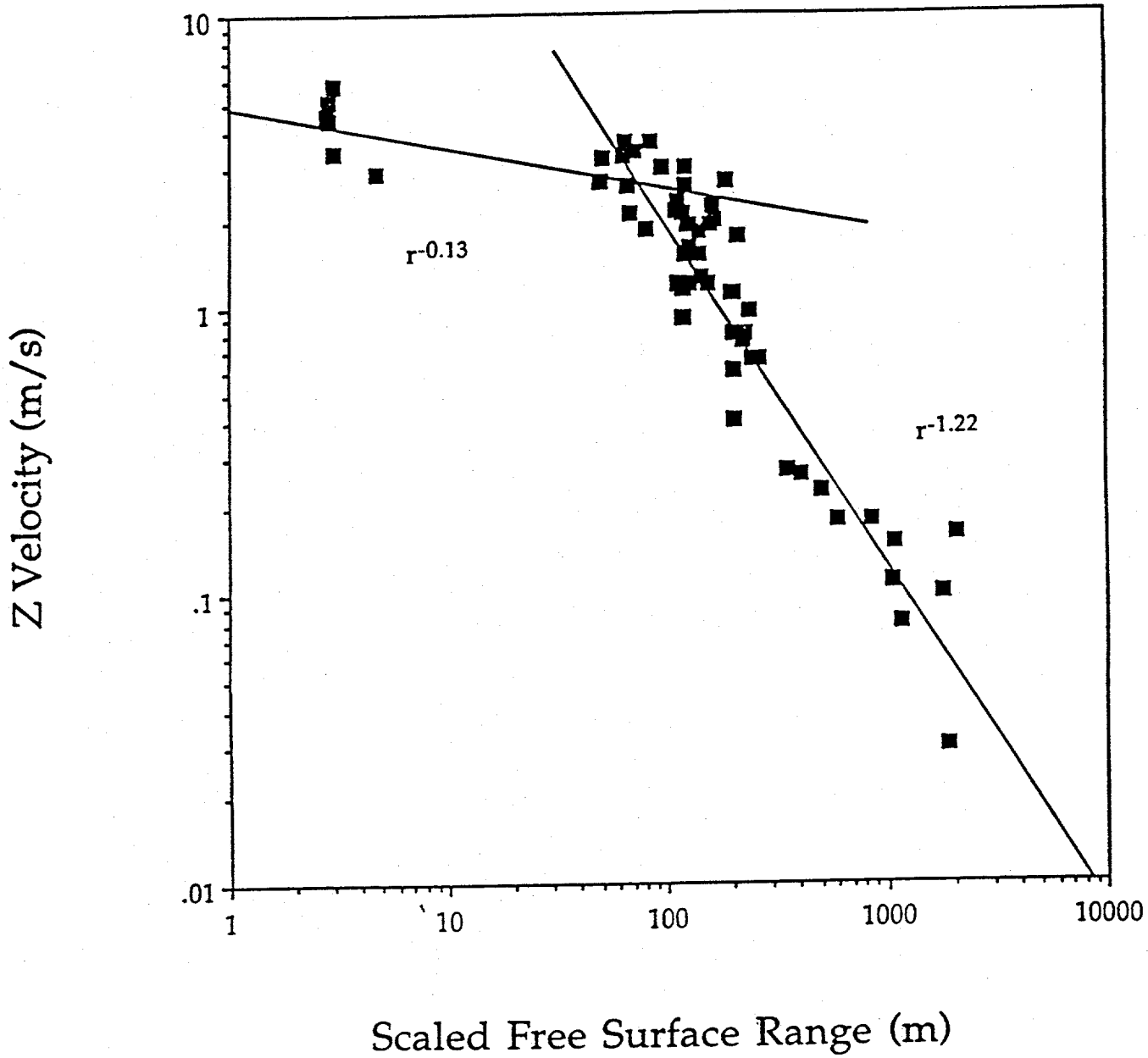

Figure 10b: The log of peak velocity versus the log of scaled free surface range for Pahute Mesa data. Power law models were fit to the data for ranges less than and greater than 100 $m/kt^{1/3}$.

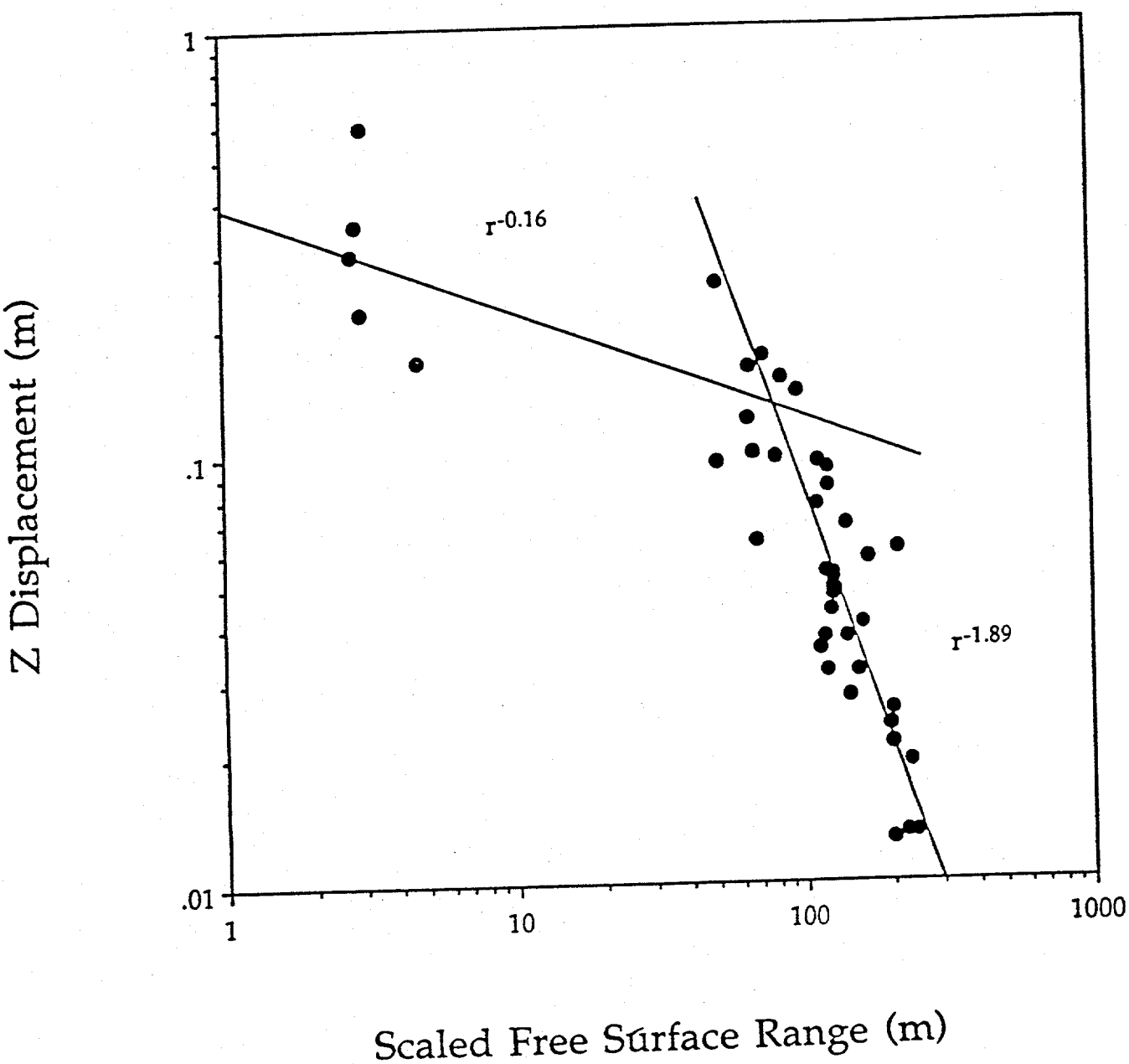

Figure 10c: The log of scaled peak displacement versus the log of scaled free surface range for Pahute Mesa data. Power law models were fit to the data for ranges less than and greater than 100 $m/kt^{1/3}$.

VERTICAL AND RADIAL VELOCITY COMPARISON

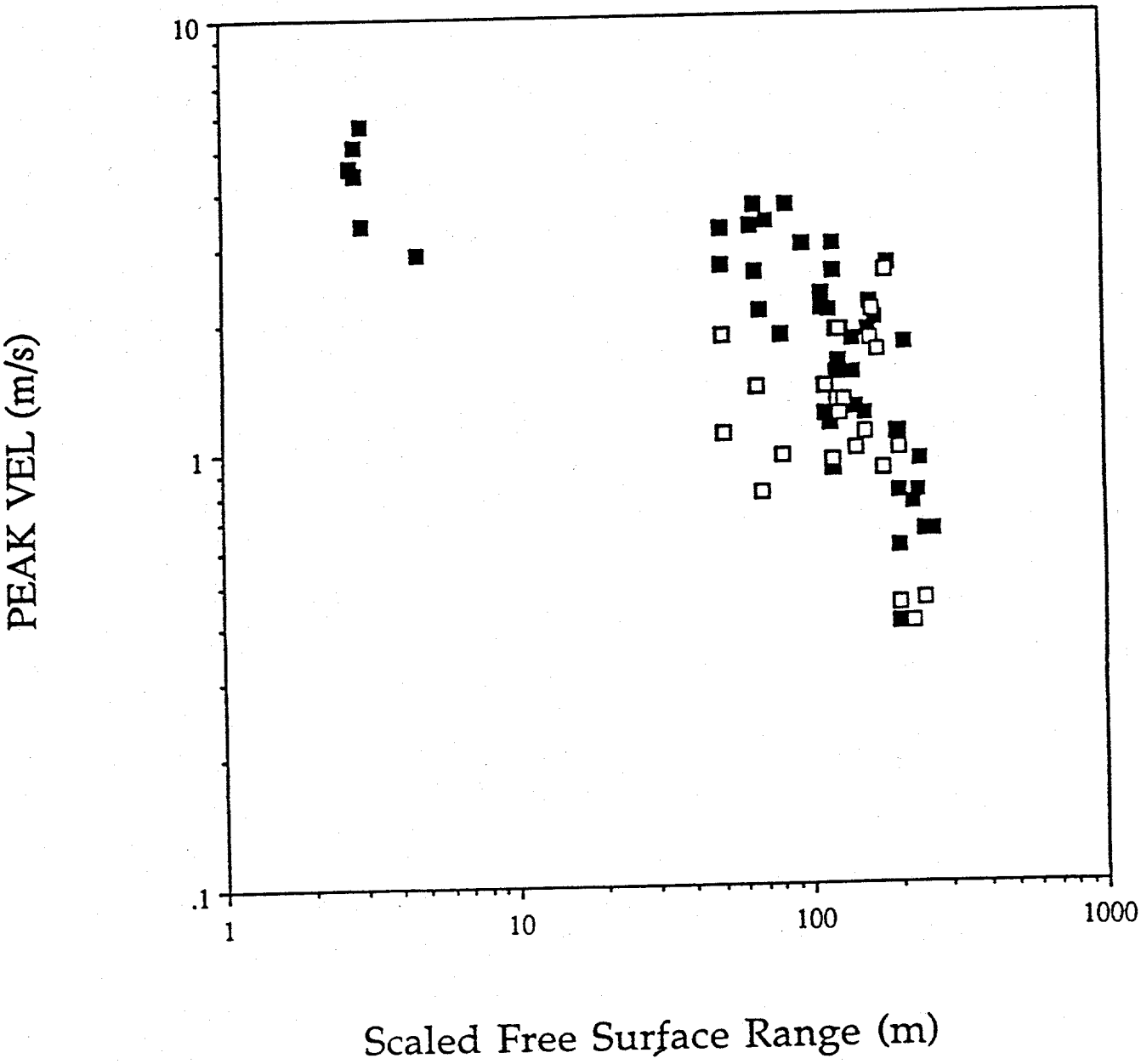

Figure 11: Comparison of peak vertical and radial velocities from Pahute Mesa nuclear explosions.

Free Surface Velocity

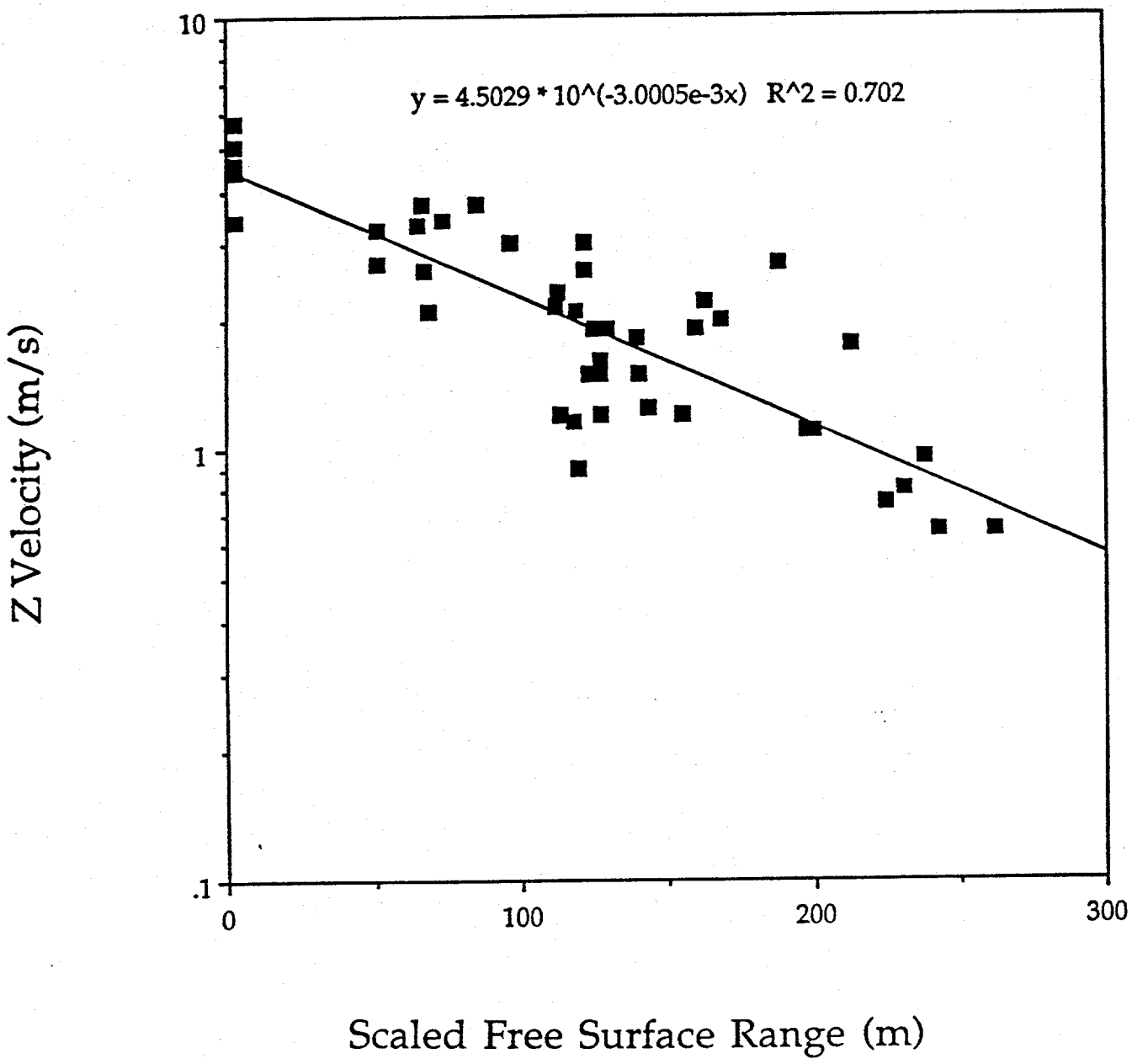

Figure 12: Fit of an exponential model (free surface range) to peak vertical velocity data from Pahute mesa.

Free Surface Velocities

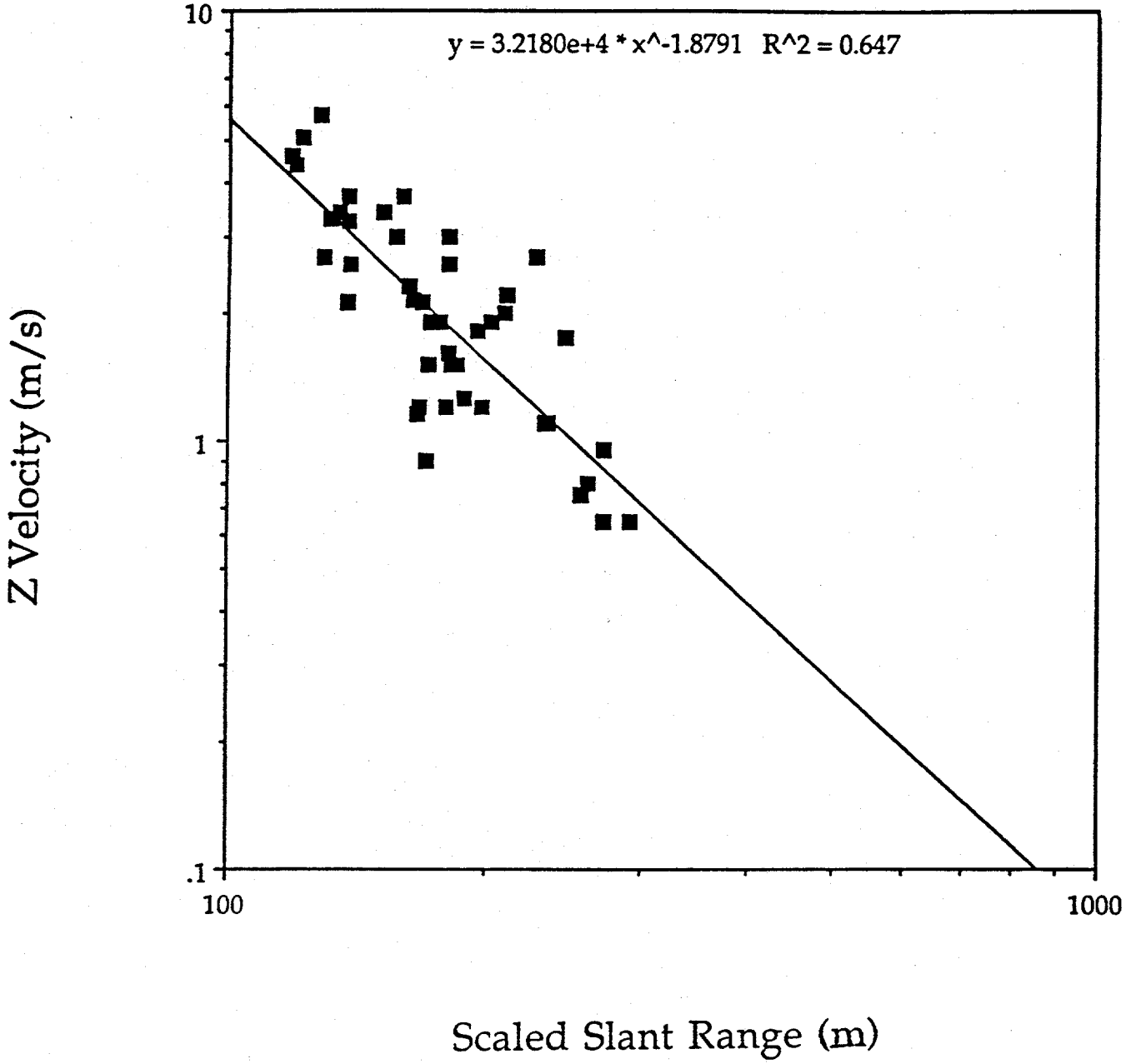

Figure 13: Fit of a power law model (slant range) to peak vertical velocity data from Pahute Mesa.

offset ($r<100m/kt^{1/3}$) the GZ range emphasizes the free surface effects and at greater offsets ($r>100m/kt^{1/3}$) r approaches R thus capturing the free-field decay and avoiding biased parameter estimates. The SSR interpretation of decay values also fits the data and synthetics although for examples shown the decay values are larger than those using SFSR. An exponential model of amplitude decay across the free surface provides the poorest fits to both synthetic and observational data.

The implication of the reduced decay region near GZ is that this region might account for a significant portion of the total spall momentum. The importance of this region to total momentum is further enhanced by the fact that most spall models predict the region directly beneath GZ to spall to greatest depth.

The more rapid spatial decay in data beyond $100m/kt^{1/3}$ is found to be near $r^{-1.96}$ for acceleration, $r^{-1.22}$ for velocity and $r^{-1.89}$ for displacement. Decay values for dry tuff published by Perret and Bass give a decay value for acceleration of -1.93, velocity -1.98, and displacement -2.2. All three estimates from the Pahute Mesa free surface data are smaller than those of Perret and Bass for free-field data.

IMPLICATIONS/CONCLUSIONS

Acceleration and derived velocity, displacement, and dwell time measurements from underground nuclear explosions above the water table at Pahute Mesa have been summarized. Free surface data contain evidence for both free surface interactions and general free-field decay rates. Free surface effects dominate to $100m/kt^{1/3}$ while free-field effects are seen at greater ranges. Acceleration, velocity, and displacement decay rates at these farther ranges are consistent with results of Perret and Bass although somewhat smaller than actual values published by these authors. This difference may reflect emphasis of vertical data in this study. Synthetic waveforms from an average Pahute Mesa velocity model replicate observed spatial decay.

Spall zone velocities, displacements, and dwell times are investigated for consistency with gravitational effects. The data is in agreement with the functional form of theoretical models although observed displacements may be as much as a factor of two to four greater than the model predicts for observed velocities and dwell times. These differences may reflect the continuous nature of the spall process and/or the role of material strength in these phenomena.

Scaling relations for free surface spall ground motions have been shown to depend on the physical model and appropriate data presentation. The form of the data presentation is implicitly linked to the appropriate physical model for wave propagation in this region around the explosion. The geometry of the problem where the source depth is comparable to the propagation distance further complicates the interpretation and comparison of results from different authors. A simple model is proposed which includes free-field attenuation of the wavefield coupled with free surface reflection coefficients. This model suggests that spall data should be plotted against FSR (r) and interpreted in term of two different decay rates. The decay of the data at close ranges, GZ to approximately 1 DOB (for routine underground events at NTS) is controlled by the free surface boundary conditions while data beyond is dominated by the free-field attenuation. Data extending to scaled free surface ranges of 1000m or beyond are necessary to constrain the second part of the model.

Since the free surface reflection is a geometrical effect, its scaling may diverge significantly from cube root of yield if standard DOB's are not used. Therefore, interpretation of the spall zone data especially in the free surface range of 0-100m is dependent upon knowledge of the source depth.

Observational data support the proposed model. Model refinement involves the inclusion of the effects of spherical wavefronts and layering in and around the

source. Data is needed in the free surface range from GZ to 1DOB to constrain the free surface interaction and out to 1000 m to constrain the free-field attenuation model. This second requirement assumes that there is no change in the free-field attenuation rate between 300 m (where most of the LANL data base stops) and 1000m.

As noted in the introduction of this paper a limited, near source ground motion data set has been explored in this study. The complexity of interpreting such data has been illustrated. The results suggest that additional data analysis is needed for events above the static water table (SWL) in Yucca Flats and for events below the SWL in both Yucca Flats and Pahute Mesa. This extended study will provide constraints on the effects of both material properties and SWL on spall zone motions.

ACKNOWLEDGMENTS

This report was supported by the Source Region Program at the Los Alamos National Laboratory for the U.S. Department of Energy under contract W-705-ENG-36 and DARPA, F19628-89-K-0025, as monitored by the Phillips Laboratory.

REFEREBCES

Bernreuter, D. L., E. C. Jackson, and A. B. Miller, 1970. Control of the dynamic environment produced by underground nuclear explosions, in Proceedings of Symposium on Underground Nuclear Explosions, 14-16, January 1970, Las Vegas, Nevada, Report Conf-700101, Vol. 2, 979-993.

Day, S. M., and K. L. McLaughlin, 1991. Seismic source represenation for spall, submitted **Bull. Seism. Soc. Am. 81**, 191-201

Day, S. M., N. Rimer, and J. T. Cherry, 1983. Surface waves from underground explosions with spall: Analysis of elastic and nonlinear source models, **Bull. Seism. Soc. Am. 73**, 247-264.

Eisler, J., and F. Chilton, 1964. Spalling of the earth's surface caused by underground nuclear explosions, **J. Geophys. Res. 69**, 5285.

Koch, K., and B. W. Stump, 1990. Observed and synthetic far-regional seismograms with implications for seismic source functions from explosions with spall, **Seismological Research Letters 61**.

Muller, G., 1985. The reflectivity method: A tutorial, **J. Geophys. 58**, 153-174.

Patton, H. J., 1990. Estimates of spall mass and spall impulse from observed strong ground motions on Pahute Mesa, submitted to **Bull. Seism. Soc. Am.**

Perret, W. R., and R. C. Bass, 1975. Free-field ground motion induced by underground explosions, Sandia Laboratories, Albuquerque, NM, 87115, SAND74-0252.

Rawson, G., 1989. Effects of in-situ stress and fracture spacing on ground motion and spall from underground nuclear explosions, Proceedings of the DOE/LLNL Symposium on Explosion-Source Phenomenology, Lawrence Livermore National Laboratory, Lake Tahoe, California, 14-16 March, 1989, CONF-890398, 75-91.

Rinehart, J. H. S., 1959. Spalling and large blasts, Proceedings of the 2nd Plow Share Symposium, San Francisco, May 13-15, 1959, Part I, UCRL-5675, 135-155.

Schlittenhardt, J., 1991. The effects of spall on teleseismic P-waves: an investigation with theoretical seismograms, AGU Monograph on Explosion Phenomenology (in press).

Sobel, P. A., 1978. The effect of spall on m_b and M_s, Teledyne Geotech Report, SDAC-TR-77-12, Dallas, Texas.

Stump, B. W., 1985. Constraints on explosive sources with spall from near-source waveforms, **Bull. Seism. Soc. Am. 75**, 361-377.

Stump, B. W., and R. E. Reinke, 1984. Spall observations and mechanisms in alluvium, **J. Geophys. Res. 89**, 11495-11506.

Taylor, S. R., J. T. Rambo, and R. P. Swift, 1991. Near-source effects on regional seismograms: An analysis of the NTS explosions PERA and QUESA, **Bull. Seism. Soc. Am. 81**, 2371-2394.

Taylor, S. R., and G. E. Randall, 1989. The effect of spall on regional seismograms, **Geophys. Res Letters 16**, 211-214.

Viecelli, J. A., 1973. Spallation and the generation of surface waves by an underground explosion, **J. Geophys. Res. 78,** 2475-2487.

Wheeler, V. E., and R. G. Preston, 1968. Scaled free-field particle motions from underground nuclear explosions, Lawrence Radiation Laboratory, University of California, UCRL-50563.

Young, G. B., and L. W. Braile, 1976. A computer program for the application of Zoeppritz's amplitude equations and Knott's energy equations, **Bull. Seism. Soc. Am. 66**, 1881-1885.